*sustainability*

MDPI

*Article*

# Analysis of the Geomechanical Phenomena That Led to the Appearance of Sinkholes at the Lupeni Mine, Romania, in the Conditions of Thick Coal Seams Mining with Longwall Top Coal Caving

**Dacian-Paul Marian * and Ilie Onica ***

Department of Mining Engineering, Mining Surveying and Constructions, University of Petroșani, 332006 Petroșani, Romania

* Correspondence: dacianmarian@upet.ro (D.-P.M.); onicai2004@yahoo.com (I.O.)

**Abstract:** Thick coal seam no. 3, block V, Lupeni mine was mined by longwall top coal caving (LTCC). After the coal mining, the ground surface underwent continuous subsidence, but since 2008, three sinkholes have appeared on the surface with important dimensions, atypical for the geo-mining conditions in this coal basin. This article is a synthesis of the study meant to decipher the geo-mechanical phenomenon that led to the emergence of these sinkholes and highlighting the main factors that contributed to the development of this phenomenon. For this purpose, measurements were made on the terrain deformations using photogrammetric methods and aerial laser scanning, when modeling with 3D finite elements, in elasto-plasticity and with the help of the Knothe–Budrik influence function. The factors that contributed to the occurrence of discontinuous subsidence phenomena are shallow mining depth, the LTCC mining method, and the presence of faults in the vicinity of the mining panels. Additionally, the geo-mechanical phenomena of subsidence terrace development and sinkholes in the mining subsidence troughs at the Lupeni mine were described.

**Keywords:** coal mining; longwall top coal caving; subsidence; chimney caving; sinkhole; aerial laser scanning; influence function; finite element method

check for updates

**Citation:** Marian, D.-P.; Onica, I. Analysis of the Geomechanical Phenomena That Led to the Appearance of Sinkholes at the Lupeni Mine, Romania, in the Conditions of Thick Coal Seams Mining with Longwall Top Coal Caving. *Sustainability* **2021**, *13*, 6449. https://doi.org/10.3390/su13116449

Academic Editor: Lucio Di Matteo

Received: 19 May 2021
Accepted: 2 June 2021
Published: 6 June 2021

**Publisher's Note:** MDPI stays neutral with regard to jurisdictional claims in published maps and institutional affiliations.

**Copyright:** © 2021 by the authors. Licensee MDPI, Basel, Switzerland. This article is an open access article distributed under the terms and conditions of the Creative Commons Attribution (CC BY) license (https://creativecommons.org/licenses/by/4.0/).

## 1. Introduction

Following the extraction of a volume of useful mineral substance from a deposit, under certain geomining conditions, continuous or discontinuous subsidence may occur at the ground surface. Continuous subsidence is characteristic of troughs and is mainly specific to the exploitation of coal deposits or, generally, to deposits of sedimentary genesis. Discontinuous subsidence is characterized by large surface displacements and the formation of discontinuities in the surface profile and may develop suddenly or progressively [1]. As the volume of underground excavation increases, the subsidence area increases until the pieces of broken rock manage to fill the underground voids. In situations where the height of the caved zone is greater than the depth of the excavation, sinkholes may appear in the form of chimney or funnel caving. Otherwise, when the thickness of the hard rock mass is greater than the height of the caved zone, then a fracture zone will appear above it [2]. In the case of mining close to the surface, sinkholes can occur during or after the excavation. Sinkholes are connected with a mass deficit. The original cavity is partially filled (partial collapse) and later possibly completely filled (full collapse) by rock mass or soil under gravitational load. The sinkhole develops from the excavation upwards until it reaches the surface [3].

Some of the forms of discontinuous subsidence are the following: crown holes, pillar collapse, chimney caving, piping, or funneling [1]. In general, these phenomena occur in the case of the exploitation of ore deposits, because of the geological conditions of ore deposits and mining methods used in metal ore mines [4].

Shallow bord and pillar coal mining is often associated with extensive subsidence and/or sinkholes on the surface due to the high percentage of extraction from mines operating at shallow depth [5]. A significant frequency of occurrence of sinkholes has been found in coal mines in Poland following the exploitation of coal deposits located at depths below 100 m, with low dip and strongly tectonized [6–8].

Dimensions and peculiarities of the sinkhole type deformations are influenced by the depth of the excavations, properties of rock masses, seams' characteristics, dimensions of the underground excavations (especially their width), voids' filling material, number of excavations located on the seams of the package, excavations located in aquifer areas, and excavations near faults that cause fractures to open [9]. According to Arkuszewski [10], sinkholes may occur in the following situations: the movement of rock masses due to underground excavations situated close to the surface; the movement of rock masses determined by the excavations located near the faults—the reactivation of the caved rocks from the old goafs; collapses around shafts; endogenous fires occurring in the remnants of coal seams located at shallow depths; and overlapping the mined edges of several coal seams.

If the column of rocks to the surface, located above an underground excavation, consists of geological formations with low cohesion, a wedge-shaped depression may develop at the ground surface; determined by the dislocation of the rock massif after a funnel, it narrows continuously in depth. It is also possible for funnels to appear due to the breaking of rock layers, and the caved material can extend bell-shaped to the depths. If rock removal or a slip occurs, a chimney caving may occur [11].

Paleo-sinkholes appeared mainly in limestone rocks. For the occurrence of paleo-sinkholes, the simultaneous presence of the following factors is necessary: karst cavities formed in calcareous rocks, such as limestone, dolomite, and gypsum, and groundwater infiltration into karst rocks [12].

In 2011, an extensive dewatering program was initiated at the lignite open-pit in Çöllolar, located in southeastern Turkey, which led to the progressive development of four sinkholes as a consequence of the untimely collapse, over a period of approximately 120 days from the start of the dewatering process [13].

Often, during mining excavations near the faults, they become active, causing destructive phenomena of the ground surface, such as fault fractures and sinkholes [2]. These ground surface subsidence phenomena in the form of sinkholes, under the influence of direct and reverse faults, taking into account the position of the underground excavations, were also studied in the case of coal mines in Great Britain [14,15]. During coal mining, some accidents, such as coal–gas outbursts, roof falling and water, and breakout could be related to reactivated faults as well. Additionally, some linear damages on the surface in the mining area, such as surface steps, crown holes, and fissures, could be induced by reactivated faults directly or indirectly [16]. The mechanisms involved in reactivating mining-induced faults were examined by Donnelly [15,17]. Such reactivation during coal mining with longwall faces is essentially controlled by several interdependent geological and mining factors. Geological factors influencing fault reactivation include the predominant and pre-existing stress state, geological history of faults, geotechnical properties distributed along the faults (friction angle, cohesion, and pore water pressure), proximity to the ground surface, local hydrogeological regime, and incidence and orientation of discontinuities in the adjacent rock masses [15,17]. The mining factors that influence the reactivation of the faults are the mining depth, the mine configuration and the geometry of the faults, the horizontal distance of the mining workings at the fault, the mining advancement speed, the mined thickness, the exploitation history, and the mining intensity of the coal deposit [15,17].

Harms and Konietzky [3] emphasize that the stability analysis of sinkholes is based on several analytical and numerical methods. The analytical methods are grouped into (a) simple geomechanical methods and (b) methods that take into account the balance of volumes. Numerical methods commonly used to simulate subsidence phenomena and

sinkholes are the finite element method (FEM), finite difference method (FDM), and discrete element method (DEM), including particle flow code (PFC). Parise and Lollino [18], from the numerical models made, found that, under certain conditions, natural caves can lose their stability, reaching the ground surface, thus inducing the appearance of sinkholes. Numerical analyses were done using both the finite element method for geological settings represented by continuous soft rock mass and the distinct element method for jointed rock mass conditions. Lokhande [19] developed numerical models using FLAC3D and 3DEC to understand the mechanism of the sinkhole subsidence under development and depillaring conditions, considering the geometry, properties of the rocks, and the sequence of extraction.

These destructive phenomena determine the removal of the lands from the economic circuit and implicitly the reduction of their value [2] and the destruction of surface constructions [20,21]. Types of collapses range from single immature sinkholes to multiple mature sinkholes, all of which may pose a significant risk to the public [22]. In this respect, the effects mining activities have on the surroundings receive significant global attention due to the nature of their environmental and social responsibilities [23]. In addition to the destruction of lands and buildings, these geomechanical phenomena have caused a significant negative impact on the environment such as the impossibility of reusing the land for construction and agriculture, disturbance of the groundwater flow regime and the hydrostatic level, emanations in the atmosphere through cracks and fissures of methane gas (with greenhouse effect) and gases from the spontaneous combustion of coal, etc. [20,21]. Additionally, the destruction of some buildings owned by disadvantaged families resulted in the appearance of special social phenomena [20,21,24,25].

Compared to the geomechanical phenomena of surface mining deformation, known from the literature, the phenomenon of sinkholes at the Lupeni mine is unique worldwide, especially due to the geo-mining conditions of the coal mine (depth of exploited panels, tectonics, and LTCC mining). The purpose of the research summarized in this article is to decipher the phenomenon of sinkhole production and the conditions of their formation in order to predict the phenomena that may occur in other similar conditions in the Jiu Valley coal mining basin. These sudden geomechanical phenomena can cause significant material damages and endanger people's lives. Therefore, if possible, in areas with a potential for sinkholes, the necessary measures should be established to reduce their negative impact.

## 2. Geology of the Lupeni Coal Deposit, Jiu Valley Basin, Romania

The Lupeni mining perimeter is delimited by the Vulcan and Paroșeni perimeters to the east and to the west by the Bărbăteni perimeter.

The deposit in this mining perimeter Lupeni (Figure 1) is higher than the adjacent areas due to the morphology of the base formations. In general, the syncline structure with the more developed northern flank is maintained. It is compartmentalized into blocks due to a generally N–S oriented fault system. The direction of the layers is generally NE–SW, with a dip reaching between 5° and 70° (lower in the central area). The perimeter is delimited to the N and S by the northern marginal fault and by the Jiu river fault, which marks the limit of the metamorphic formations of the Getic or autochthonous domain, with the Ruppelian deposits. To the west, there is a tendency for the crystalline formations to overlap. In addition to the major disjunctive elements, a series of transversal and longitudinal faults were highlighted in the perimeter, with the NNW–SSE direction and inclinations towards E, which compartmentalize the deposit into seven main blocks.

In the Lupeni mining field, through the mining works of prospecting, exploration, and exploitation, the main tectonic blocks were delimited and 21 coal seams were identified, formed from coking coal from the Jiu Valley basin. The coal seams that have economic importance are no. 3, 4, 5, 8/9, 13, 14, and 15, which were exploited between the horizons 800 m ÷ 300 m, with variations from seam to seam.

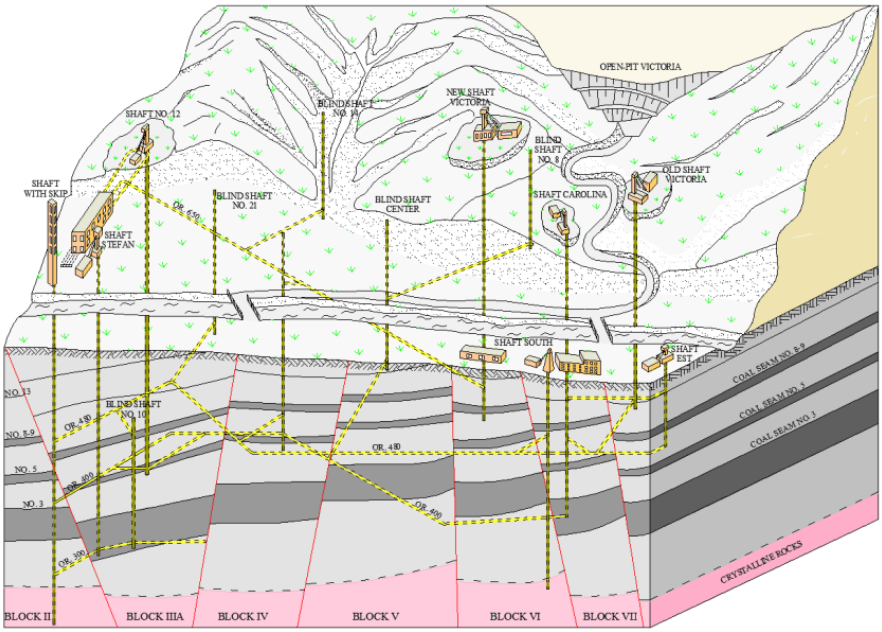



**Figure 1.** Block diagram of the Lupeni mining perimeter (not to scale).

Coal seam no. 3 presents the greatest economic importance in the Jiu Valley basin and implicitly in the Lupeni mining field. This thick coal seam is located 20–50 m from the Ruppelian–Chattian boundary. It has a thickness that varies from 40 m, in the northern area, to 10 m, in the area of the Jiu river pillar and the Lupeni town. It consists of several coal banks with clay intercalations. The roof of coal seam no. 3 consists of clayey and calcareous sandstones and striped, well layered, and blackish sandstone clays, rich in fossiliferous flora and frequent sideritic concretions. The floor is made of compact black sandstone and fine sandstone clays, with spherosideritic concretions.

The coal deposit from the Lupeni perimeter has a high geological complexity, being intensely tectonized and presenting large variations of qualitative and quantitative parameters. Hard coal from the Lupeni mining perimeter is coking, with moderate agglutination-coking properties.

The average physical–mechanical and elastic characteristics of coal seam no. 3 and the roof rocks are presented in Table 1.

**Table 1.** Average values of physical, mechanical, and elastic characteristics of coal seam no. 3 and roof rocks—Lupeni mine.

| Name | Apparent Specific Weight, $\gamma_a \cdot 10^4$, [N/m$^3$] | Compressive Strength, $\sigma_{rc}$ [MPa] | Tensile Strength, $\sigma_{rt}$ [MPa] | Cohesion, $C$ [MPa] | Internal Friction Angle, $\phi$ [°] | Elasticity Modulus, $E$ [MPa] | Poisson's Coefficient, $\nu$ |
|---|---|---|---|---|---|---|---|
| Coal | 1.31 | 9.5–18.0 | 0.8–1.3 | 1.1–2.5 | 49–58 | 530–1600 | 0.17 |
| Immediate roof rocks | 2.58 | 44.1 | 5.6 | 6.0 | 50 | 5100 | 0.2 |
| Main roof rocks | 2.609 | 128.0 | 13.2 | 20.5 | 54 | 5500 | 0.12 |

## 3. Evolution of Coal Seam Mining from the Lupeni Mine

The Lupeni mine represents the mining perimeter with the largest extension in the basin, whose activity of hard coal extraction began in 1892. At present, at the Lupeni mine, specific works are being carried out for the final closure of the mine.

The coal seams in the package located above coal seam no. 3, no. 4, 5, 8, 9, 13, 14, 15, and 18, have been exploited in different periods of time, and the time elapsed since the completion of the exploitation of these coal seams, until now, is 30 years for coal seam no. 5, 34 years for coal seam no. 13, and 39 years for the rest of the coal seams in the package. The actual exploitation of these strata, by the complete caving of the roof rocks, lasted for

a period of 20–25 years. This leads us to the immediate conclusion that the caved rocks existing in the goafs of these coal seams had a long enough time to settle [26], and their contribution to surface deformation can be ignored in this study.

At the ground surface at the Lupeni mine, in the area of block V, there have been, since 2008, a series of three sinkholes with important sizes: sinkhole SH1 (Figure 2a) on 22 April 2008, at the limit with the mining panel P6; sinkhole SH2 (Figure 2b) on 19 May 2014, next to the panel P10; and sinkhole SH3 (Figure 2c) on 19 June 2018, at the limit with the panel P9. The three sinkholes that appeared in the subsidence profile of the Lupeni mine (which, usually in the case of mining operations in the Jiu Valley, have a continuous character) are totally atypical for these coal mines and very rarely found in coal mines, in the world, located in the same conditions.

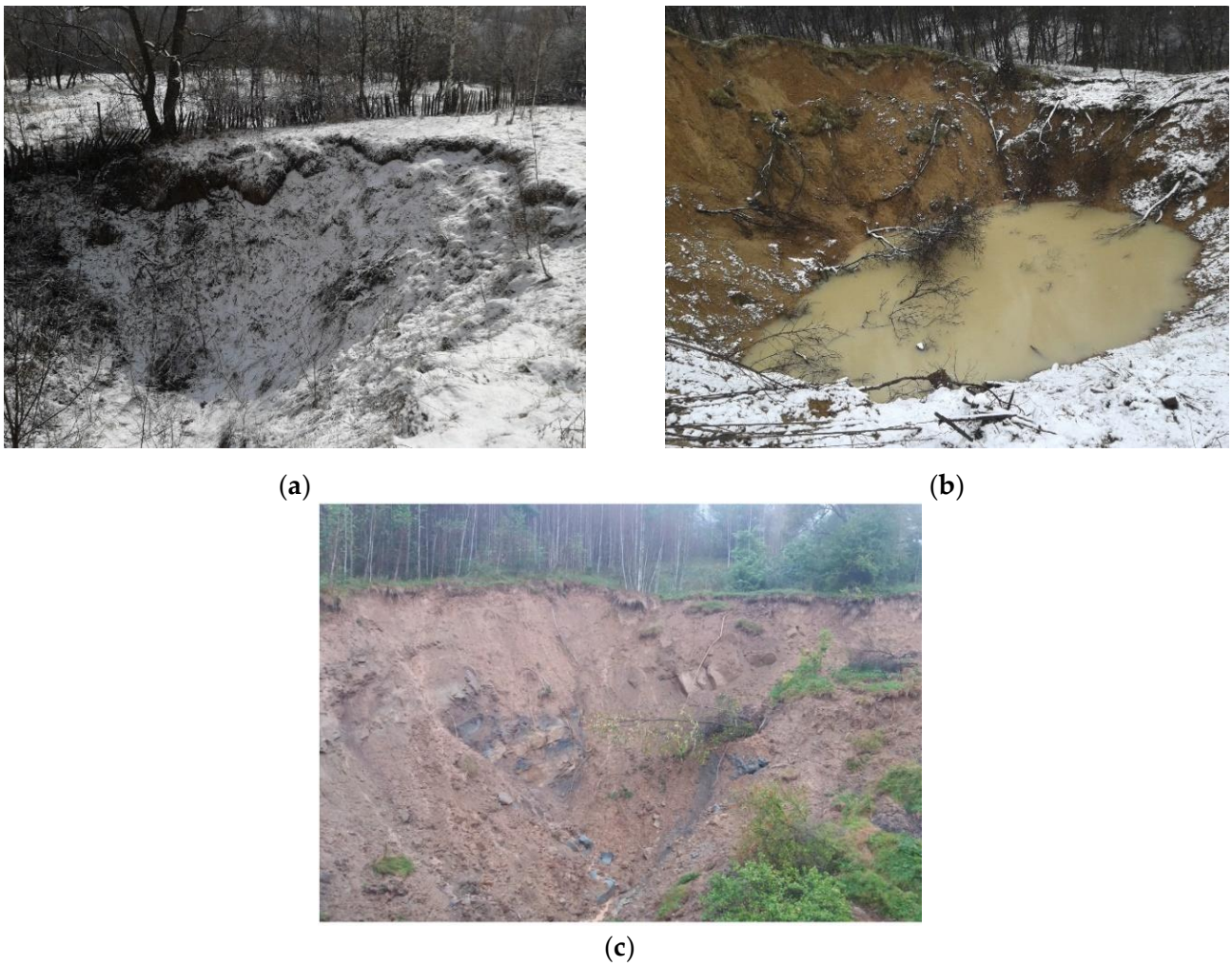


**Figure 2.** Photos with sinkholes—Lupeni mine: (**a**) sinkhole SH1 (22 April 2008); (**b**) sinkhole SH2 (19 May 2014); (**c**) sinkhole SH3 (19 June 2018).

These phenomena of discontinuous subsidence are produced in block V, at the Lupeni mine, in the conditions of longwall top coal caving mining of thick coal seam no. 3, equipped with a classic technology (coal cutting by drilling–blasting, individual roof support composed of hydraulic props and articulated caps, and transport with armored face conveyors).

After the extraction of the roof coal seams, the exploitation of the deposit continued with the extraction of coal seam no. 3, with longwall top coal caving faces (Figures 3 and 4). The last mined panels on coal seam no. 3, block V, involved in the appearance of sinkholes were panels P6, P9, P7, and P10, located at an average depth of 242–275 m. Mining panels

P6, P10, and P9 were in operation at the date of the appearance of the respective sinkholes, having the main features presented in Table 2 and Figure 5.

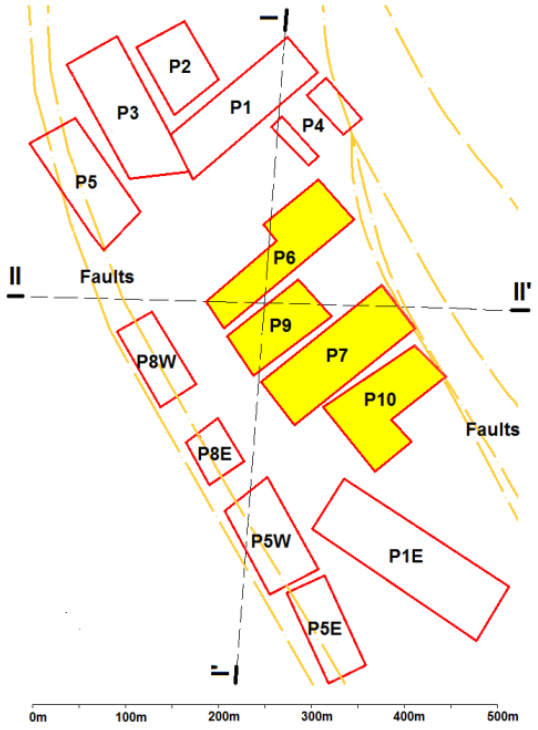
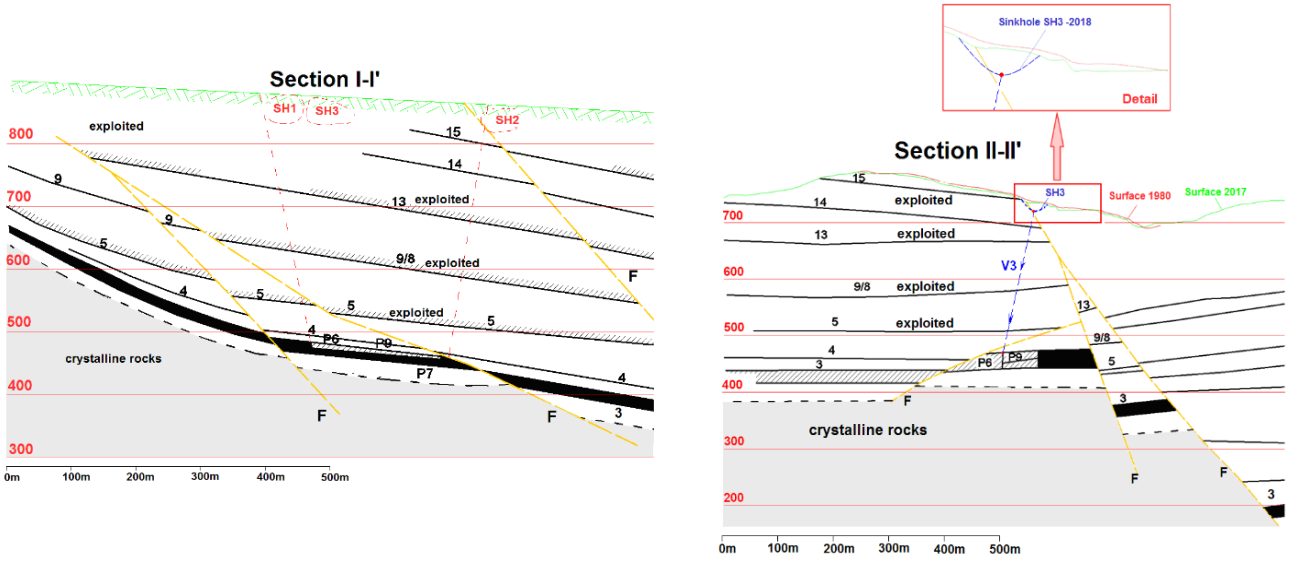



**Figure 3.** Plan view with the mining panels from coal seam no. 3, block V, Lupeni mine (from the end of 2018).




(**a**) (**b**)

**Figure 4.** Vertical cross-sections through the plane in Figure 3: (**a**) Vertical section I-I'; (**b**) Vertical section II-II' 3,4, . . . , 15–coal seam number; P6, P7, and P9—mining panels; SH1, SH2, and SH3—sinkholes; F—faults; V3—vector/axis of sinkhole.

**Table 2.** The main features of mining panels P6, P9, P7, and P10 and of the corresponding sinkholes SH1, SH2, and SH3, in the area of coal seam no. 3, block V, Lupeni mine.

| No. | Features | Sinkhole No. 1 | Sinkhole No. 2 | Sinkhole No. 3 |
|---|---|---|---|---|
| | | Panel P6 | Panel P10 | Panel P9 |
| 1 | Mined length of the panel at the time of sinkhole appearance, (m) | 89.8 | 102.4 | 74.1 |
| 2 | Length of longwall coal face, (m) | 60/37 | 50/87 | 53 |
| 3 | Coal slice mining height, (m) | >12–15 | >15–22 | >12–15 |
| 4 | Average mining depth, (m) | 265 | 242 | 275 |
| 5 | Date of operation start | 1 May 2005 | 1 September 2012 | 1 January 2017 |
| 6 | Date of appearance of the sinkhole/chimney caving | 22 April 2008 | 19 May 2014 | 19 June 2018 |
| 7 | Sinkhole diameter, (m) | 32.9 | 37.8 | 51.7 |
| 8 | Sinkhole depth, (m) | 11.6 | 12.8 | 18.8 |
| 9 | The distance from the coal face to the corner of the pillar at the time of sinkhole appearance, (m) | 12.2 | 25.8 | 74.1 |
| 10 | The distance from the panel to the fault system, (m) | 26 | 6 | 82 |

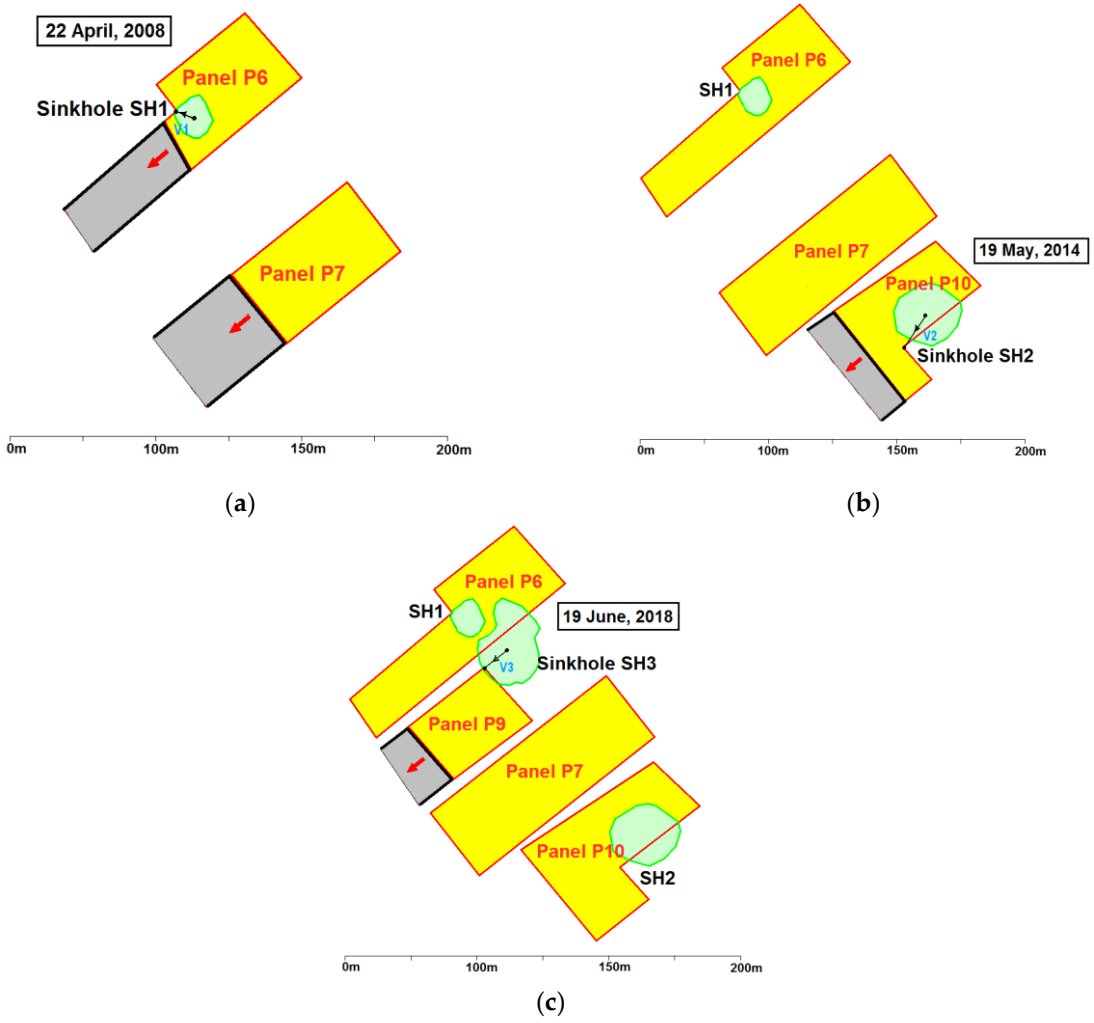



**Figure 5.** Layout plan of mining panels P6, P7, P9, and P10 at the time of the sinkhole's appearance: (**a**) Sinkhole SH1: 22 April 2008; (**b**) Sinkhole SH2: 19 May 2014; (**c**) Sinkhole SH3: 19 June 2018; V1, V2, and V3—vectors of gravitational displacement of caved rocks in chimneys.

The development of discontinuous subsidence phenomena at the Lupeni mine was influenced by the simultaneous presence of several geo-mining factors, and the explanation of these phenomena required the corroboration of in situ data, with the results obtained from calculations, and the experience of research on similar phenomena appeared worldwide.

## 4. Material and Methods

### *4.1. Evaluation of the Deformation in Time of the Ground Surface, in the Lupeni Mine Perimeter, Monitored with the Help of Photogrammetric Measurements and by Aerial Laser Scanning*

The evaluation of the ground surface deformation, under the influence of the underground mining of coal seam no. 3, was performed for a period of approximately 38 years, between 1980–2018. For this, the ground surface configuration from 1980, determined by aerial photogrammetry, was compared with the ground surface from 2017, obtained by aerial laser scanning.

In order to evaluate the subsidence during the analyzed period, two digital elevation models (DEM) were generated, corresponding to the years 1980 and 2017, the total vertical displacement of the surface being obtained by the difference between the values corresponding to the two models.

Three types of terrain elevation models are known, namely DSM (digital surface model), DEM (digital elevation model), and DTM (digital terrain model) [20]. DSM is a 3D representation of the surface that contains all the objects on it (natural—trees, vegetation, etc., or artificial—buildings, bridges, pipes, etc.). DEM is a 3D representation of the surface from which all objects were removed. DTM is a 3D representation of the surface that contains the X, Y, and Z coordinates of the points stored in digital format. This type of digital model contains elevations and certain geographical elements and natural characteristics of the land such as rivers, mountain ridges, etc. A DTM is actually a DEM that has been enhanced with some additional elements to the database, such as break lines and other observations [20].

#### 4.1.1. Digitization of Old Topographic Plans and DEM Generation

In order to evaluate the deformation of the ground surface, an area of interest from the Lupeni mining perimeter was analyzed, with a total area of 293,600 $m^2$, corresponding to two aerial photograms taken in 1980 [20].

In order to obtain the DEM for the area, it was necessary to go through the following steps [20]:

- the maps have been converted from analog into digital format;
- the raster images obtained were inserted in the AutoCAD program and georeferenced on coordinates in the STEREO 70 reference system (Romania's geodetic reference system);
- the maps were digitized by vectoring the contours and elevation points;
- the file resulting from the map digitization was imported into the Global Mapper program, which was used to generate the DEM.

##### Inserting and Georeferencing Raster Images

Raster images were inserted one by one into the AutoCAD program using the Raster Design module. Inserting the raster image requires the introduction of the following parameters: the coordinates of the insertion point, the rotation angle of the photograms, the scale, the unit of measurement, and the density of points on the unit of measurement. In the case of new photograms (orthophotograms), the program automatically recognizes these parameters. In the case of old maps, these parameters must be entered manually, and if they are not known, the map is inserted manually on random coordinates, following that the raster image is georeferenced manually.

Georeferencing is the operation of assigning real coordinates and, where appropriate, spatial extensions, in order to locate the mapped area on the earth's surface. After the precision georeferencing of the raster images (in this case, on coordinates in the Jiu Valley

'58 reference system), it was necessary to pass them in the STEREO 70 reference system (Figure 6).

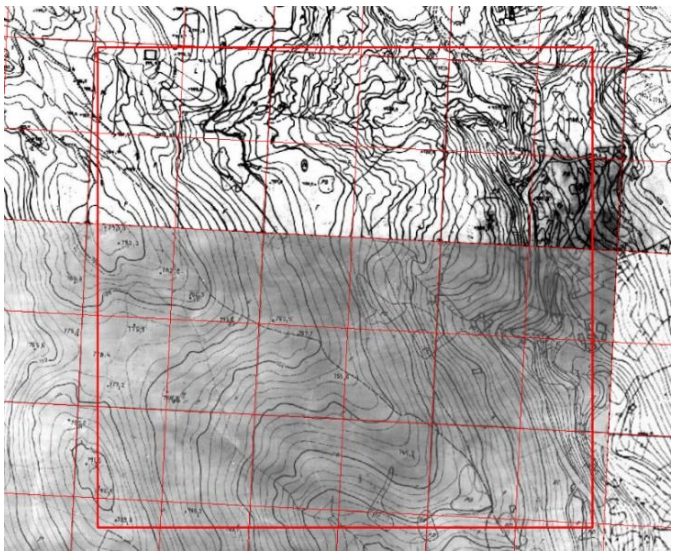


**Figure 6.** Positioning raster images on their final location.

Digitization of Topographic Plans

The digitization operation is the transition from the raster shape of maps/images to a vector shape (dots, lines) that can be used later. This transition is performed by vectorization, an operation that can be performed (1) manually, using the polyline (after following the contour of the level curve, we will have to associate the elevation of the contour to the polyline), or (2) semi-automatically, using the facilities offered by the AutoCAD Raster Design program.

For the semi-automatic vectorization of contours, raster images were first transformed from grayscale images into bitonal images. Then, we proceeded to the semi-automatic vectorization of the main level curves in the area of interest, as well as the elevation points located on the level curve planes (Figure 7). Secondary level curves were also vectorized.

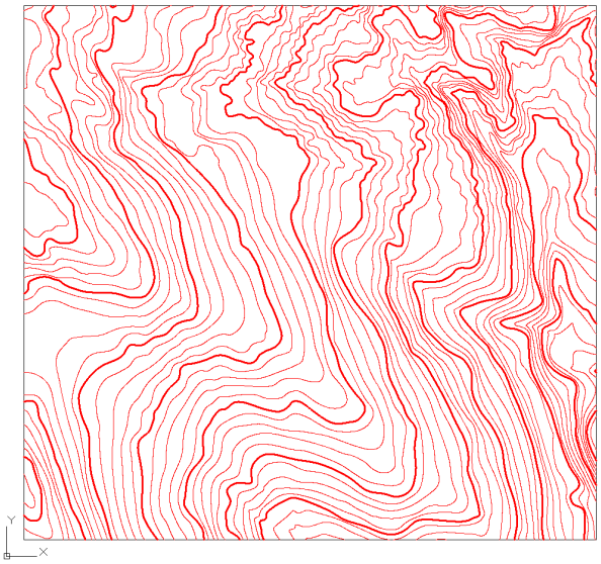


**Figure 7.** The area of interest represented in vector format.

Completion of the DEM for 1980

The elevation model of the terrain, corresponding to 1980, was made based on digitized plans using the Global Mapper program. For this, the vector format file was imported (see Figure 7) from where, in the end, the elevation model of the land corresponding to 1980 was obtained (Figure 8).

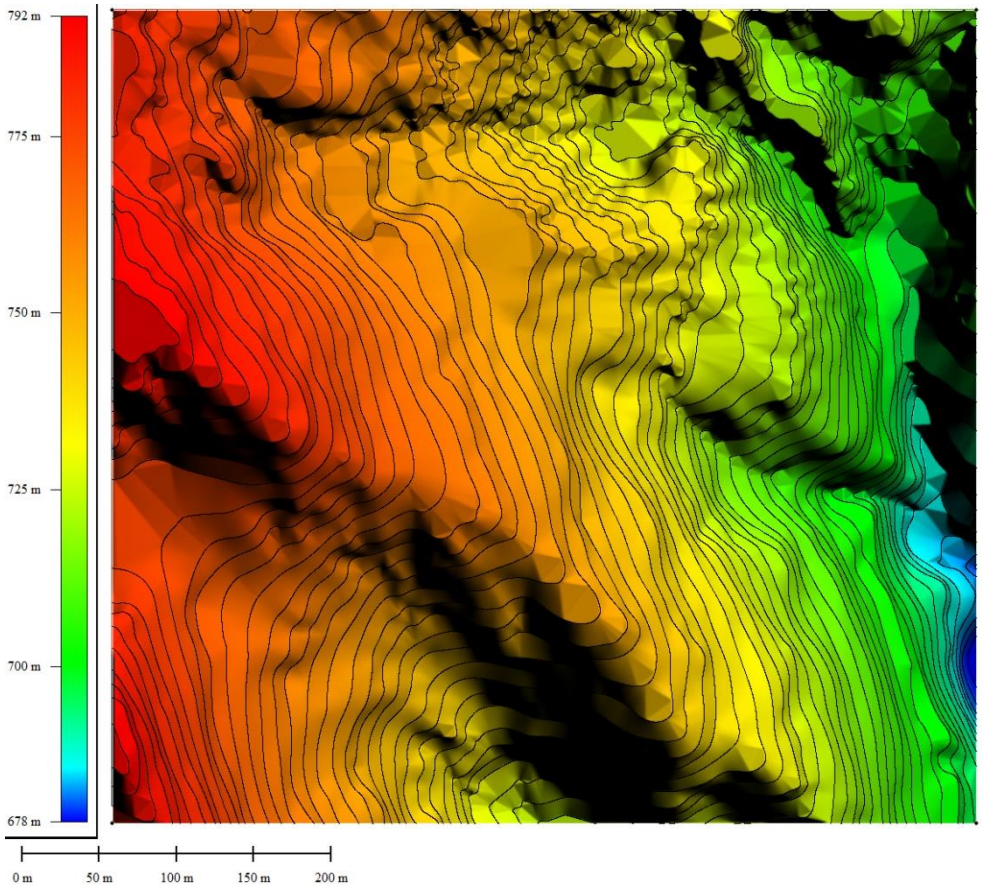



**Figure 8.** Land elevation model—1980.

4.1.2. Obtaining the DEM for 2017 through Aerial Laser Scanning

Laser scanning technology is one of the latest methods of collecting geodata, having applicability especially in areas where high-precision 3D data are used [27]. Laser scanning is a method by which a surface is measured/scanned using laser technology. It analyzes a real-world environment or object in order to collect information on its surface and possibly its appearance (for example color). The information collected can then be used to construct two-dimensional representations or three-dimensional models, which can be used in a wide variety of applications. Laser scanners are line-of-sight instruments that allow the capture and definition of spatial data (in X, Y, and Z coordinates), using signals with the laser beam reflected by the scanned objects or surfaces. 3D laser scanning technology is new in the field of topography [28]; it can be divided into two categories: static laser scanning and dynamic laser scanning.

The measurements underlying the terrain elevation model for 2017 were performed by aerial laser scanning. Based on these data and with the help of the Global Mapper program, the terrain elevation model for 2017 was generated. (Figure 9). Analyzing comparatively the two models of land elevation (for 1980 and for 2017), it can be seen that there are major differences between them, developed over a period of at least 37 years, as a result of underground exploitation the ground surface undergoing significant changes, represented

by multiple subsidence troughs, two sinkholes, and significant fissures and cracks of the ground surface.

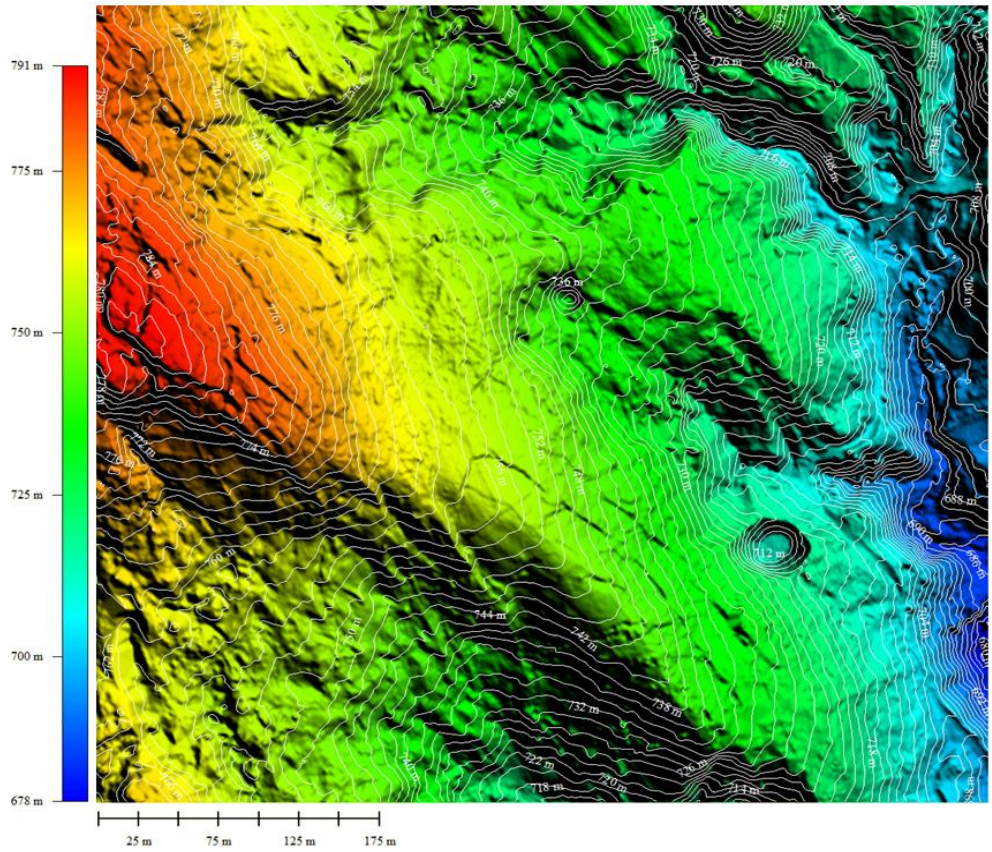



**Figure 9.** Land elevation model—24 June 2017.

*4.2. Prognosis of Surface Deformation, Using the Knothe–Budryk Influence Function Method*

The principle for subsidence prediction is based on the extraction of infinitesimal elements of area. Subsidence at any point on the surface is obtained from the sum of the influence of each extracted element, using the principle of superposition [29]. The superposition of the effects, specific to the method of influence functions, is very useful in the case of studying the subsidence troughs produced by the exploitation of several neighboring panels.

In order to predict the displacements that occurred at the surface of block V, from the Lupeni mine, as a result of the underground exploitation of thick coal seam no. 3, the influence function elaborated by Knothe (also known as Knothe-Budryk theory) was applied. This method is based on the Gaussian distribution of probabilities [7,30–33]: This method, represented by Knothe's theory, assumes that the influence function for the two-dimensional case, applied to a point with maximum subsidence, located vertically, is given by [33]:

$$g(x,s) = \frac{S_0(x)}{r} \cdot \exp\left[-\pi \cdot \frac{(x-s)^2}{r^2}\right] \quad (1)$$

where:

$r$ is the radius of principal influence: $r = h/\tan\beta h$—the overburden depth;
$\beta$—the angle of principal influence ($\beta = 57°$);
$s$—the coordinate of the point, P, where subsidence is considered;
$x$—the coordinate of the infinitesimal excavated element;

$S_0(x)$—the convergence of the roof of the infinitesimal excavated element:

$$S_0(x) = m(x) \cdot a(x);$$

$m(x)$—the extraction thickness;

$a(x)$—the roof convergence (subsidence) factor ($a(x)$ = 0.8, for roof control by top coal caving).

For finite excavation limits $x_1$ and $x_2$, the equation of subsidence is [33]:

$$S(x,s) = \frac{S_{max}}{r} \int_{x_1}^{x_2} \exp\left[-\pi \cdot \frac{(x-s)^2}{r^2}\right] \cdot dx \quad (2)$$

$S_{max}$ is the maximum possible subsidence (supercritical subsidence) within finite excavation limits $x_1$ and $x_2$.

Although this method is frequently used to predict the deformation of the ground surface under the influence of underground mining, it has some limitations, as certain important factors cannot be taken into account in explaining this phenomenon, such as geomechanical properties of rocks and tectonic accidents.

### *4.3. 3D Finite Element Modeling of the Stress Concentration around the Exploited Panels*

In order to evaluate the concentration of stresses in the areas of the sinkholes, from the contour of the mining panels, spatial modeling was performed, with 3D finite elements, of the exploitation stages of coal seam no. 3 at the time of the three sinkholes. The CESAR-LCPC finite element code and the CLEO 3D processor were used for this purpose.

Due to the complexity of the models and the large computational resources required, models with "mining voids" were generated, in the hypothesis of Mohr–Coulomb-type elasto-plastic behavior without hardening. For better accuracy of the results, extended models were made (with a volume of 0.683 km$^3$), with dimensions of approximately X = 1265 m, Y = 1317 m, and Z = 410 m (Figure 10).

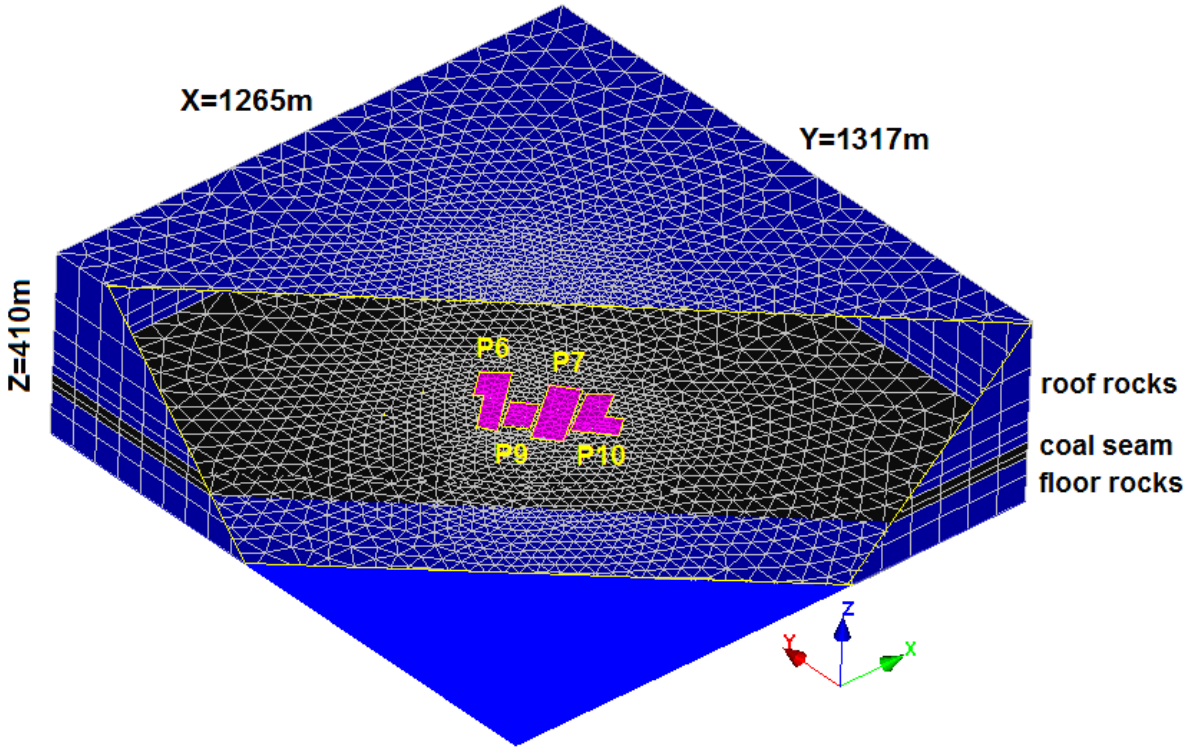



**Figure 10.** 3D finite element model—operating situation of panels P6, P9, P7, and P10, from 19 June 2018.

The discretization of the models, respective of each region, was achieved by triangular prismatic finite elements with linear interpolation, resulting in a total number of 14,600 nodes and 25,578 volume elements.

The constitutive law of behavior "elasto-plasticity without hardening" required the introduction of the following calculation parameters: apparent specific density, modulus of elasticity, Poisson's ratio, cohesion, angle of internal friction, and angle of dilatation. The actual values of the properties of the rocks in the massif are normally different from those obtained in laboratory tests (see Table 1). The modulus of elasticity, cohesion, and tensile strength is generally considered to be 0.1–0.25 of the results of laboratory tests. The Poisson's ratio is adopted to be about 1.2–1.4 in laboratory tests. These properties are used in numerical modeling [34,35] and, in the present case, were established following analyses of their sensitivity to the variation of the main parameters of the models for the Jiu Valley coal basin [36,37].

## 5. Results

### *5.1. Evaluation of Ground Surface Deformation during 1980–2018*

In order to evaluate the surface deformation in the case of the Lupeni mine, in the period 1980–2017, the two elevation models of the ground surface were imported into the Global Mapper program. From the difference between the elevations of the two elevation plans, the vertical displacements/subsidences produced between 1980 and 2017 related to the studied perimeter were obtained. In order to obtain a more recent situation of the deformation of the terrain, to the measurements from 2017 were added those performed on the sinkhole that appeared on 19 June 2018 (Figure 11).

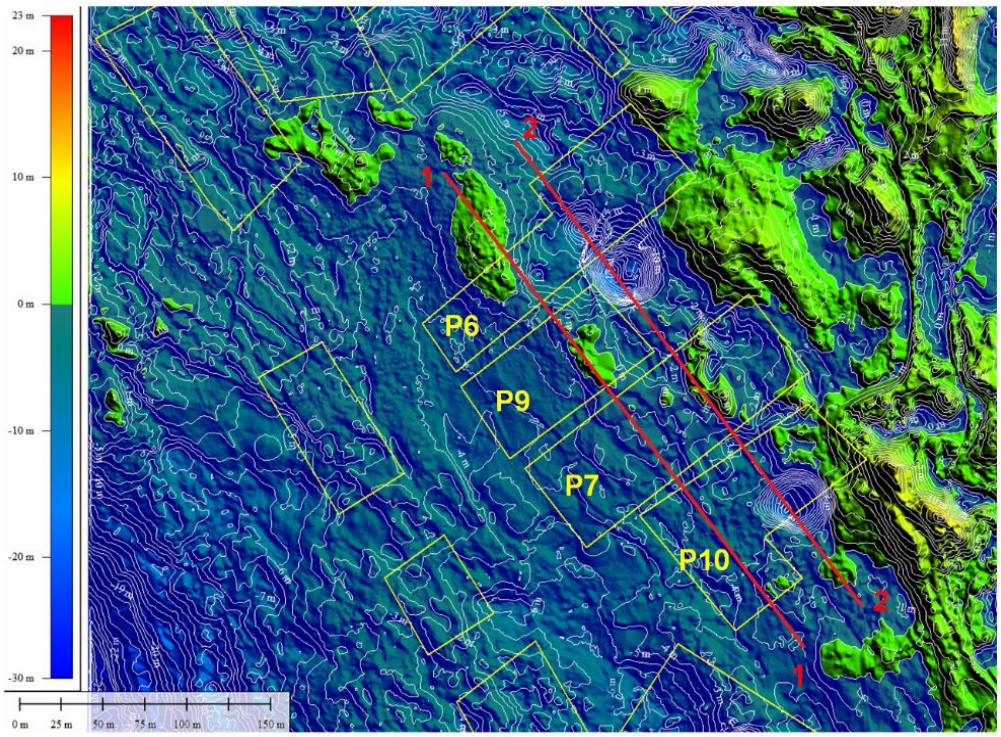



**Figure 11.** Scalar representation of ground surface subsidence on 19 June 2018, in sinkholes perimeter [20].

Figure 12 plots the ground surface subsidence, in two representative sections, in the areas affected by the sinkhole phenomena.

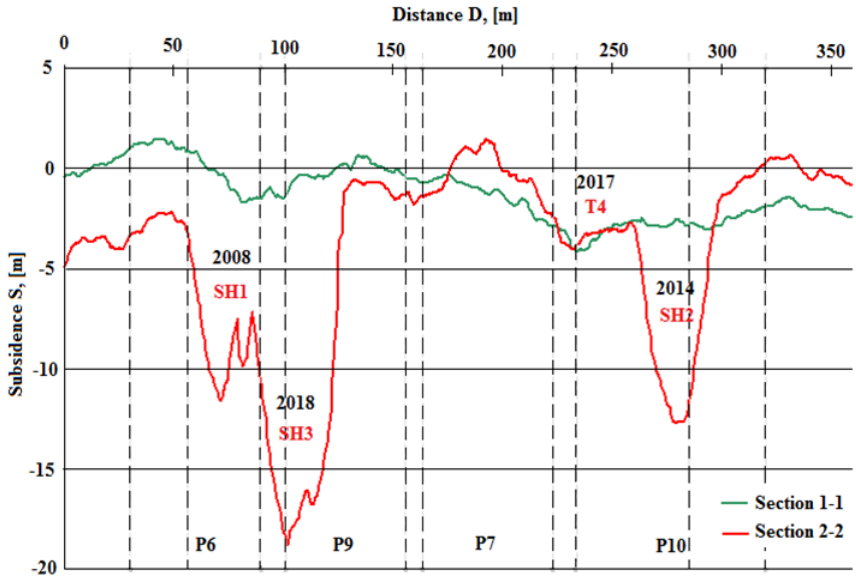



**Figure 12.** Subsidence on the alignments—panels P6, P9, P7, and P10: Vertical cross-section 1-1; Vertical cross-section 2-2 (sinkholes SH1, SH2, SH3, and the subsidence terrace T4).

Maximum subsidence of the ground surface, determined in the middle of the panels, constituting the object of the present study, in 2017, is contained in Table 3.

**Table 3.** Maximum subsidence in the middle of the panels, in 2017.

| Maximum Subsidence, in mm | | | |
|---|---|---|---|
| **Panel P6** | **Panel P9** | **Panel P7** | **Panel P10** |
| 6000 | 1400 | 2000 | 4200 |

In the geo-mining conditions of the exploited panels, maximum subsidence is between 1400 mm, for the case of panel P9 and 6000 mm, for panel P6, and the dimensions of the three sinkholes and the subsidence terrace are summarized in Table 4.

**Table 4.** The dimensions of the sinkholes resulting from the measurements from 2018.

| Sinkhole | | | | | | Subsidence Terrace | |
|---|---|---|---|---|---|---|---|
| **SH 1** | | **SH 2** | | **SH 3** | | **T 4** | |
| **Depth, (m)** | **Diameter, (m)** | **Depth, (m)** | **Diameter, (m)** | **Depth, (m)** | **Diameter, (m)** | **Depth, (m)** | **Diameter, (m)** |
| 11.6 | 32.9 | 12.8 | 37.8 | 18.8 | 51.7 | 5.1 | 30 |

In both of the sections presented above (Figure 12), as well as from the photographs in Figure 2, it results that the sinkholes appeared on the surface of a rugged relief and the shape of the surface pits, resulting as a consequence of the sinkholes, changed by associating them with the landslide phenomenon.

### *5.2. Assessment of Surface Deformation in the Case of the Lupeni Mine, Using the Knothe–Budryk Influence Function Method*

For the realization of this prediction, using the Knothe–Budryk influence function method, only the panels exploited on coal seam no. 3, located in the area of interest in the vicinity of sinkholes, were considered. For this purpose, an area with dimensions of 1400 m × 1750 m was delimited, and the distance between the points used in the calculation of the land surface displacement was 25 m. Applying, with the help of Excel and

AutoCAD programs, the method of Knothe–Budryk influence functions, taking into account the superposition of the effects, for the case of the mining panels studied from block V, from the Lupeni mine, resulted in the scalar representations of vertical displacements from Figures 13 and 14.

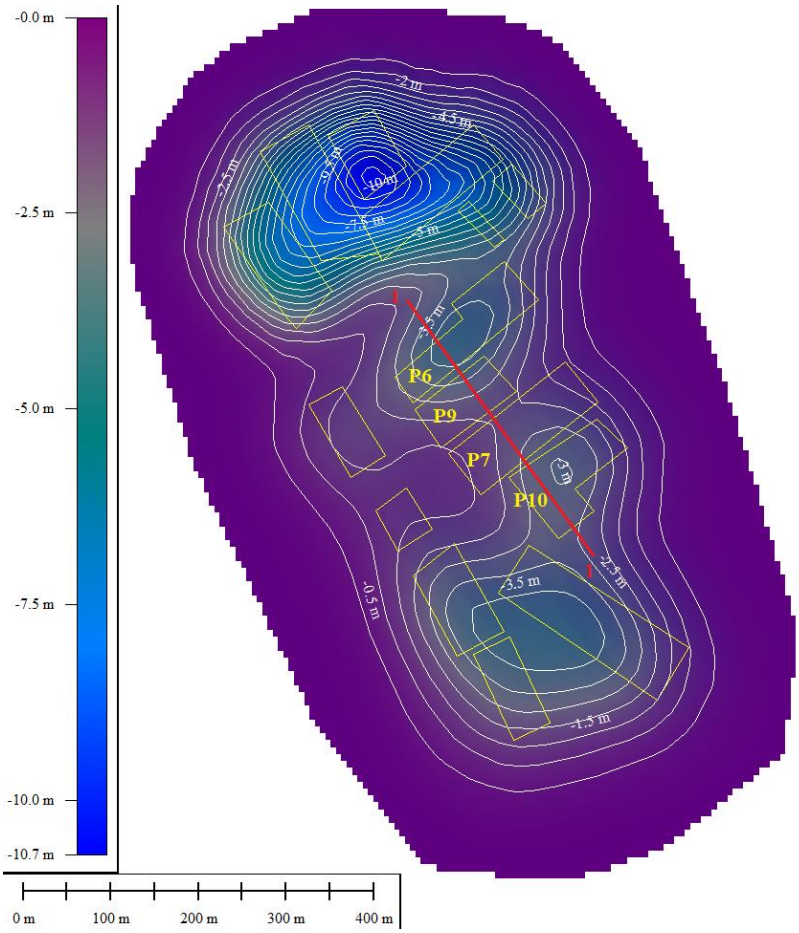



**Figure 13.** Scalar representation of predicted subsidences using the Knothe–Budryk influence function method.

Analyzing the shape of the subsidence troughs using the influence function, it can be seen that, under the conditions of mining of the panels considered, some composite troughs appeared on the surface, obtained by overlapping the effects of operation of adjacent panels. In areas where, in reality, sinkholes have appeared on the ground surface, in the case of the prognosis obtained with the help of the influence function, a continuous subsidence trough has resulted, with maximum subsidence between 2.5 and 3.9 m (Figure 13).

For the area of panels P6, P9, P7, and P10, which are interesting from the point of view of the present study, the forecasted maximum values of the ground surface subsidences are summarized in Table 5.

The obvious differences between the measured subsidence curve and the curve of the calculated one using the influence function are due, in particular, to the fact that the ground surface subsidence phenomena were associated with landslides, the initial terrain relief being rugged (see Figure 8). These landslides ended with accumulations of volume in certain areas of the ground surface (see Figure 11). Given that the geological formations covering the coal deposit are made of alluvial rocks, these geomechanical phenomena (mining subsidence combined with landslide) are very complex and cannot be simulated with the help of influence functions. Moreover, the influence functions cannot predict the appearance of sinkholes.

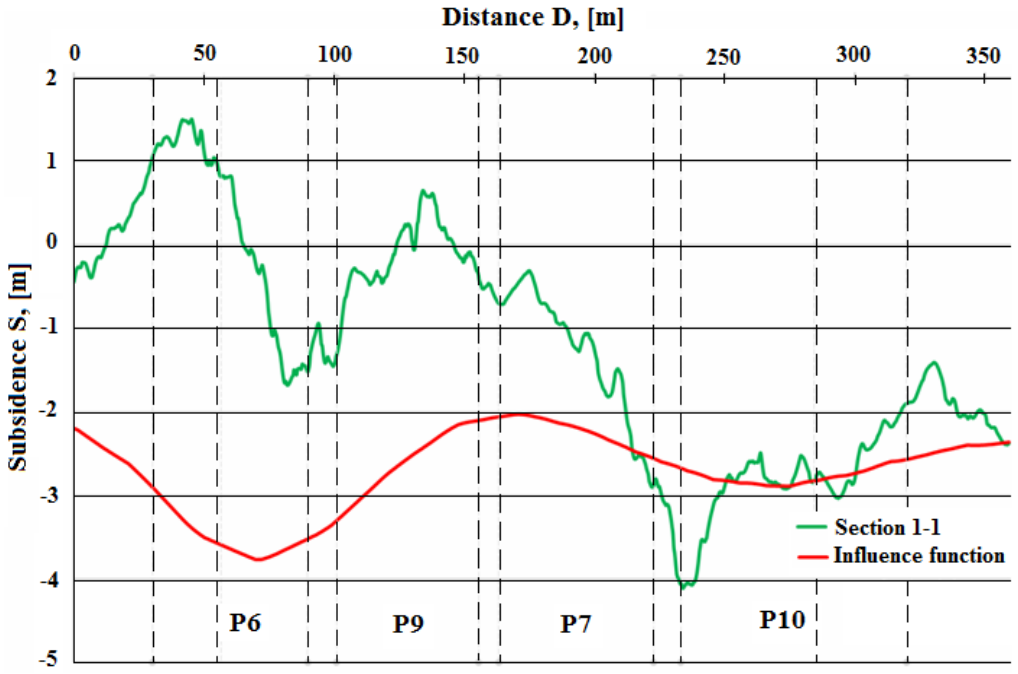



**Figure 14.** Representative vertical Section 1-1 through the subsidence troughs, predicted using the Knothe–Budryk influence function method (see Figure 13) and measured (see Figure 11).

**Table 5.** Maximum ground surface subsidence, in the middle of panels P6, P9, P7, and P10, from the Lupeni mine, using the Knothe–Budryk influence function.

| Panel | P6 | P9 | P7 | P10 |
|---|---|---|---|---|
| Maximum subsidence, $W_{max}$, in mm | 3900 | 2500 | 2500 | 3100 |

## 6. Discussion

### *6.1. Factors That Influenced the Occurrence of Discontinuous Subsidence Phenomena in Block V at the Lupeni Mine*

For the geo-mining conditions at the Lupeni mine, the following main factors were analyzed, which led, cumulatively, to the appearance of sinkholes:

- shallow depth location of underground excavations, approximately 242–275 m;
- the movement of large volumes of rocks from the roof, in a relatively short period of time, due to the exploitation of high-height slices (approximately 12–25 m), by the longwall top coal caving mining method;
- the movement of rock masses according to the fault planes (faults reactivation), determined by the underground excavations located near them, at distances of 6–82 m, from the first fault, and of the coal faces at a distance of 108–156 m, from the fault when the sinkhole phenomenon starts;
- concentration of stresses on the edges of the pillars, between the exploited panels, especially on the corner areas of the pillars.

If only one factor stated above was missing, the sinkholes from the Lupeni mine would not have occurred, at least in the shape and amplitude at which they occurred.

#### 6.1.1. Mining Depth of Coal Seam No. 3, Block V, Lupeni

The operation location depth is very important in this study because:

- it directly determines the natural state of stresses in the massif and indirectly, the stress-induced state, at the level of the exploitation and influences the behavior of the rocks around the excavations;

– relative to the height at which the deformations are transmitted above the excavations, it determines the degree of influence of the stability of the ground surface and the geo-mechanical behavior of the rock mass.

The stresses found in the rock mass are grouped, depending on the origin, into natural stresses, which are found in the intact massif, and induced stresses, which are the result of stresses changes due to mining excavations [38]. The value of the initial stresses calculated at the level of panels P6, P9, P7, and P10, for the depth range of 242 and 275 m, is between $6 \times 10^3$ and $6.9 \times 10^3$ kN/m$^2$ for vertical stresses $\sigma_v$ and $1.45 \times 10^3$ and $1.65 \times 10^3$ kN/m$^2$ for horizontal stresses $\sigma_h$.

From Table 2, it is found that the dimensions of the pits (depth and diameter) are in ascending order, depending on the time of appearance of the sinkholes: SH1, SH2, and SH3. From Figure 5, it can be seen that the number of panels exploited with each appearance of a new sinkhole is increasing and implicitly is increasing the state of stresses and deformations developed in the rock massif (due to the increase in the total volume of mining voids). This shows that the volume of the pits depends, among other things, on the state of stresses that appeared in the rock massif at the time of the production of each sinkhole.

From the 3D finite element analysis of the exploitation stages from the moment of the appearance of each sinkhole, an increase of the vertical stresses in the areas on the contour of the panels is found in the vicinity of the sinkholes, from $1.51 \times 10^4$ kN/m$^2$, in the case of the first sinkhole SH1, at $1.88 \times 10^4$ kN/m$^2$ in the case of sinkhole SH2, and then at $1.91 \times 10^4$ kN/m$^2$ under the conditions of the third sinkhole SH3.

#### 6.1.2. The Geomechanical Behavior of the Coal Face and the Roof Rocks

Panels P6, P9, P7, and P10, at the level of coal seam no. 3, were extracted by the longwall top coal caving mining method [39,40]. In this case, the projected thickness of the mining slice was between 12 and 25 m, which is unlikely to have been achieved in practice (in reality being much higher), due to the impossibility of controlling the discharge of top coal caved.

All three caving pits occurred during the mining of the panels: P6, sinkhole SH1; P10, sinkhole SH2; P9, sinkhole SH3. Therefore, it can be pointed out that the phenomenon of sinkholes was triggered in the goafs of the panels where the movement of the rocks was not completely stabilized. These phenomena occurred at a relatively short distance from the coal face (between 12.2 and 74.1 m, see Table 2), where the rocks moved continuously inside motion ellipsoids [39].

In general, following the exploitation of a coal seam, the state of stresses developed in the surrounding rocks changes and is accompanied by deformations, failures, and displacements of rocks, with variable intensities, depending on the area of influence of the goafs and the factors that govern the stability of the massif.

The state of stresses and strains developed in the case of longwall faces with top coal caving is similar to that of roof control by integral roof rocks caving. Thus, according to Figure 15, six important areas can be delimited around the longwall faces with top coal caving [41]:

Zone I starts at 20–30 m in front of the longwall coal face, the state of stresses being specific to a massif with elastic behavior, having a value approximately equal to that of the natural state of stresses.

Zone II, immediately in front of the coal face, develops up to 20–30 m, depending on the rigidity of the roof rocks, and has the value of approximately $(2 \div 3) \cdot \gamma \cdot H$, which makes the top coal above the longwall face intensely cracked, depending on the coal strength and the mining speed of advancement. On the first 2–3 m, the concentration of stresses is maximum, causing the pronounced cracking of the coal and its transition from an elastic behavior to elastic–plastic and then visco-plastic, near the coal face. The fracturing of the top coal, produced in this area, will then help to extract it by gravity, without the need to use explosives.

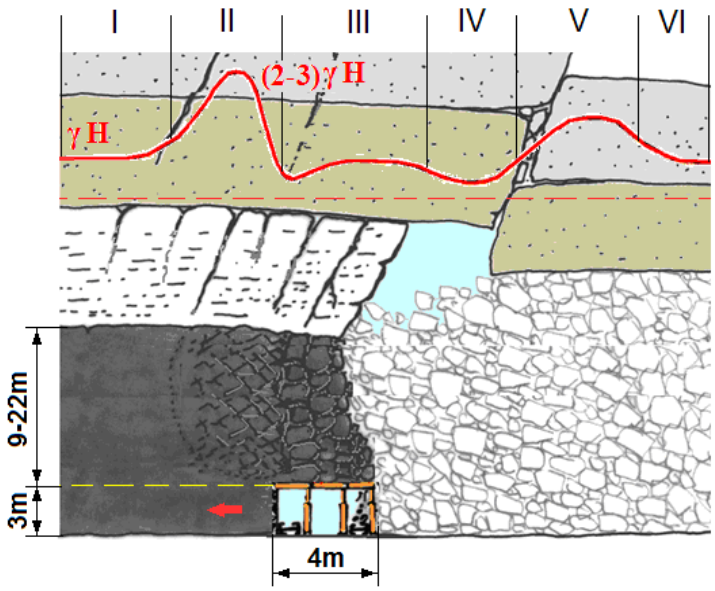



**Figure 15.** Stress state around the longwall face with top coal caving.

Further, the de-stressing of the top coal will lead to the reduction of the mining pressure transmitted by the roof rocks on the face support, in zone III of stresses on the longwall face, below the value of the natural stresses.

In zone IV, starting from the boundary behind the coal face, there is an intense movement of the caved rocks and the top coal, in the form of motion ellipsoids, generated in the phase of evacuation of the caved top coal, which leads to the reduction of stresses to less than one-third of their initial value.

Outside the area of movement of the caved rocks behind the longwall face, they begin to gradually settle in zone V, constituting a support for the roof rocks, redistribution, and concentration of 1.5–2.0 times the initial stresses in the massif. Then, progressively, starting from approximately 30–40 m, behind the coal face, in zone VI, the caved rocks behind the coal face are continuously compacted in time, determining the recovery of the initial state of stresses.

Due to the large rotational space of the roof rocks' layers, allowed by the void created by LTCC mining, the banks of covering rocks greatly affect the behavior of the top coal and the coal front [39]. In the sense of the above, the quantitative description of the main characteristics of the stress–strain state of the top coal can be summarized as follows: in the case of LTCC, the movement of the top coal starts from an area in front of the face line, at the level of the first traction plane (in general, field observations show that the starting point of the movement, in the case of low-strength coal seams, is between 15 and 20 m in front of the coal face line and 6–10 m from the coal face, for those of average strength); the main movement of the top coal in front of the coal face is horizontal, and behind the front it is vertical; the density of fractures induced in the top coal increases, the dimensions of the coal blocks decrease, and the mechanical strength characteristics of the coal gradually decrease, with the movement of the caved coal towards the exhaust window [39].

In the case of thick coal seams with low inclination, the laboratory results showed that when the mining height is 10 m, the first caving step of immediate roof rocks and separating it from the main roof rocks occurs behind the longwall face at a distance of 20 m from the starting line of the mining of panel. After that, the main roof rocks collapse periodically at intervals of 14–15 m. The total caved height of the roof rocks reaches 44 m, and the loosening coefficient of the caved rocks is 1.32–1.43 [42]. From the analysis of the structure formed by blocks or pieces of compressed rocks arranged in the form of a bridge, between the coal face areas and the goaf, and taking into account the technical

characteristics of longwall face equipment, the equilibrium structure is prone to two forms of failure, namely by sliding and by rotation [43].

The top coal begins to open its fractures at 8 m in front of the coal face, which are inclined at 60–80° to the goaf. As the coal face advances, the fractures widen and their inclination decreases; at the same time, the density of fractures increases. The distance between fractures ranges between 0.8 and 1.5 m [39].

#### 6.1.3. Fault Reactivation

The results obtained worldwide (from field observations and analytical, numerical, and rock-like materials modeling) have led to the conclusion that the reactivation of faults, located near mining excavations, can cause changes in the continuity of the surface deformation and even stimulate the appearance of instantaneous geo-mechanical phenomena, such as sinkholes [2,15].

Mining factors influencing fault reactivation are mining depth, mine configuration and faults geometry, horizontal distance of fault mining workings, mining speed, mining thickness, mining history, and exploitation intensity of deposit [15].

Additionally, from the research conducted by Donnelly et al. [15], three important ideas can be retained, namely:

1) The reactivation of the faults is simultaneous with the mining subsidence phenomena and appears due to the release of the stresses accumulated along these faults;
2) The phenomenon of reactivation of faults can cause shear displacement, leading to an uneven generation of subsidence, on both sides of faults;
3) The movement of the ground surface caused by the reactivation of faults can take place over periods ranging from weeks to years and can continue even after the mining subsidence has stopped.

From the 3D representation of the subsidences, as differences between the land elevations from 1980 and those from 2017/2018, the presence of the following phenomena can be identified:

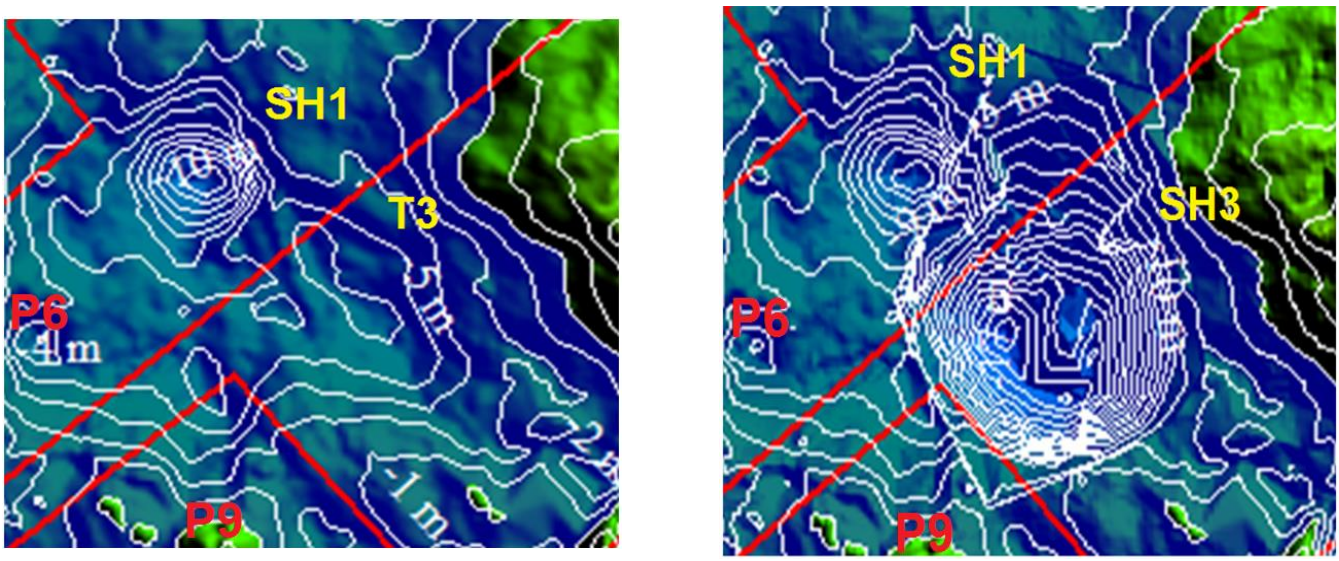
a) continuous subsidence (subsidence trough) above most exploited panels;
b) zones with maximum subsidence, developed on small areas, located along major faults, with a discontinuous appearance in the subsidence profile, in the form of a terrace, such as terraces T3 and T4 (one of which is the precursor phase T3, which anticipates the development of sinkhole SH3, appeared only in 2018);
c) sinkhole SH1 appeared in 2008, SH2 appeared in 2014, and then SH3, in 2018.

The addition of the measurements performed on the SH3 sinkhole led to the completion of the map mentioned above, and the approximate assessment of the situation of the existing surface land in 2018 (see Figures 11 and 12). Interestingly, by comparing the two planes, represented in Figure 16, the phenomenon of accentuated deformation of the ground surface is captured, before the failure of the roof rocks and the formation of the sinkhole, respectively, with the presence of the T3 terrace (Figure 16a) and after the transition of the T3 subsidence terrace into the SH3 sinkhole (Figure 16b).

These two comparative stages of the ground surface relief, from 1980 and 2017, corroborated with the layout plan of the exploitation of coal seam no. 3, constitute concrete arguments in identifying the causes that led to the appearance of sinkholes in the perimeter of the Lupeni mine.

Although most of the panels in block V were extracted by the mining method and technology with LTCC, sinkholes appeared only at the border with panels P6, P9, and P10. The question is: what geo-mining peculiarities exist in the area of these panels, in relation to the other panels exploited with the same system, which favored the appearance of discontinuities in the subsidence profile of the ground surface? Considering the alignment of a certain direction of the sinkholes and the discontinuity terraces of the diving profile, which is approximately identical to the orientation of the traces in the plane of coal seams no. 3 of major tectonic accidents, the obvious answer is the existence of the two major faults

and spatial positioning in relation to the geometry of the panels in operation with LTCC (see Figures 2–5).




(**a**) (**b**)

**Figure 16.** Dynamics of land deformation in the area of occurrence of the sinkhole SH3: (**a**) 24 June 2017—intensification of deformations in the form of T3 terrace; (**b**) 19 June 2018—the appearance of SH3 sinkhole.

The development of the three sinkholes at the boundary with the pillars between the mining panels is the consequence of the differentiated mechanism of the collapse of the rock layers in the two geological blocks delimited by these faults.

In addition to the arguments made above, cracks and fissures produced on the surface, following the phenomenon of reactivation of faults, are ways of infiltration of surface water on these planes of minimum strength. Infiltrated water causes a significant reduction in the strength characteristics of the rock massif on the fault plains (cohesion, coefficient of friction, shear and tensile strengths, etc.) by dissolving the calcareous cement (for example: from marl) and binding the water to clay minerals (such as montmorillonite from clay rocks), etc. Thus, in this context, the movement of rock masses, according to the fault plans, can be accentuated, determining the amplification of the local discontinuous subsidence phenomena and accelerating the appearance of cracks, terraces, and sinkholes in the outcrop areas of major faults.

#### 6.1.4. Concentration of Stresses on the Corners of the Mining Panels

Following the position of the three sinkholes on the exploitation plan of coal seam no. 3, a model of their placement is found near the corners of the mining panels. Additionally, in the case of the corner between Panel P7 and Panel P9, where a sinkhole has not yet appeared, there is an accentuation of the subsidence phenomenon on the surface (see Figure 16a) in the form of a T3 terrace, as an indicator of the possibility of subsequent, sudden production of a chimney caving.

It is known that the closer the mining limit is to a tectonic accident, the higher the stress concentration [44]; the sinkholes should have been as close to the fault as possible. First, the concentration of stresses on a mining corner is almost double that of a panel edge, to which is added the input brought by the presence of the fault near the corner of the pillar. This highlights the development of vertical stresses in terms of mining level, resulting from the 3D finite element model, which shows that in the corners of the pillars, the vertical stresses have the value of $1.9 \times 10^4$ kN/m$^2$ in relation to the rest of the areas on the contour, where the vertical stresses have the value of approximately $1.5 \times 10^4$ kN/m$^2$.

However, why in this location of the corners of the pillars did the sinkholes occur and not only some subsidence terraces or some more important subsidence phenomena appeared? The explanation results from the different behavior of the roof rocks from the edges of the pillars in relation to areas in the center of the goafs.

If the roof rock layers located in areas in the center of the goafs are fractured into smaller pieces and moved to the goafs, instead, to the boundaries with the pillars, the roof rock layers have a totally different behavior. At first, the rock layers above the exploitation level remain in the form of cantilevers oriented towards the goafs, which requires the marginal pillars to be crushed. Thus, the pillars are destroyed/sloping towards the exploited space; according to a plan with an inclination of approximately 50–60°, the coal thus crushed sliding towards the caved rocks in the goafs, whose lateral thrust, at least at this stage, is quite low. In fact, the destruction of the pillars between the panels is possible precisely due to their transition from the triaxial state of stress to a biaxial and monoaxial one, due to the lack of lateral thrust of the caved rocks from the goafs.

Under such conditions, at least the first rock layers, from the immediate roof, in the cantilever, break into large blocks and rotate towards the goaf, articulate with each other, and temporarily support the upper rock layers in the cantilever. The large blocks of rock in the immediate roof and the rock layers in the cantilever in the main roof are loaded to shear by the stress concentrators in the corners of the panels. When the maximum shear stresses exceed the shear strength of the rock layers, a sudden failure occurs, after a circular or elliptical cylindrical surface, followed by an instantaneous movement of the rock blocks according to the gravitational vector, inside the sinkhole, due to the cumulative compaction of the spaces between the rock blocks. The distance that the rock blocks slide, resulting in sinkholes from the surface is $h_{expl}/k_{ar}$; where $h_{expl}$ is the exploited height or the sum of the heights of the coal face and the top coal; $k_{ar}$ = 1.15 ÷ 1.2—the remaining loosening coefficient, after settling the rock blocks. In our case, 20 m/(1.15 ÷ 1.2) = (17.4 ÷ 16.7) m, values that justify depth sinkholes appearing on the surface.

The fact that the vector of the gravitational displacement of the caved rocks on the chimney caving is oriented for each sinkhole in a different direction (see Figure 5) is further evidence that these corners of the pillars are arranged at the base of the sinkholes, from underground. If, in the conditions of the different locations of the three sinkholes, at least two of the three vectors (V1, V2, and V3) were parallel, then another determining factor should have been sought.

From Figure 17, it can be immediately noticed that the stresses developed on the pillars between the panels are excessive, which calls into question the design of the pillars as undersized. More precisely, a development of maximum shear stresses is observed on the corners of the pillars $\tau_{s\,max}$ = 7.17·10$^3$ ÷ 8.96·10$^3$ kN/m$^2$, values above the coal shear strength limits in coal seam no. 3 (of approximately 1.4·10$^3$ ÷ 2.5·10$^3$ kN/m$^2$), which implicitly led to the destruction of the corners of the pillars and the sloping of their boundaries to a slope below 55–60°. This phenomenon also determined the possibility of the appearance of sinkholes, by shearing the rock layers in the form of blocks and cantilevers located in the vicinity of these corners (see Figure 18).

### *6.2. Description of the Discontinuous Subsidence Phenomena from The Lupeni Mine*

Analyzing the discontinuities in the subsidence profile, at the limit with the mining panels P6, P9, P7, and P10, we can notice the existence of two different discontinuity phenomena, namely (a) the phenomenon of terraces/discontinuity steps and (b) the phenomenon of sinkholes.

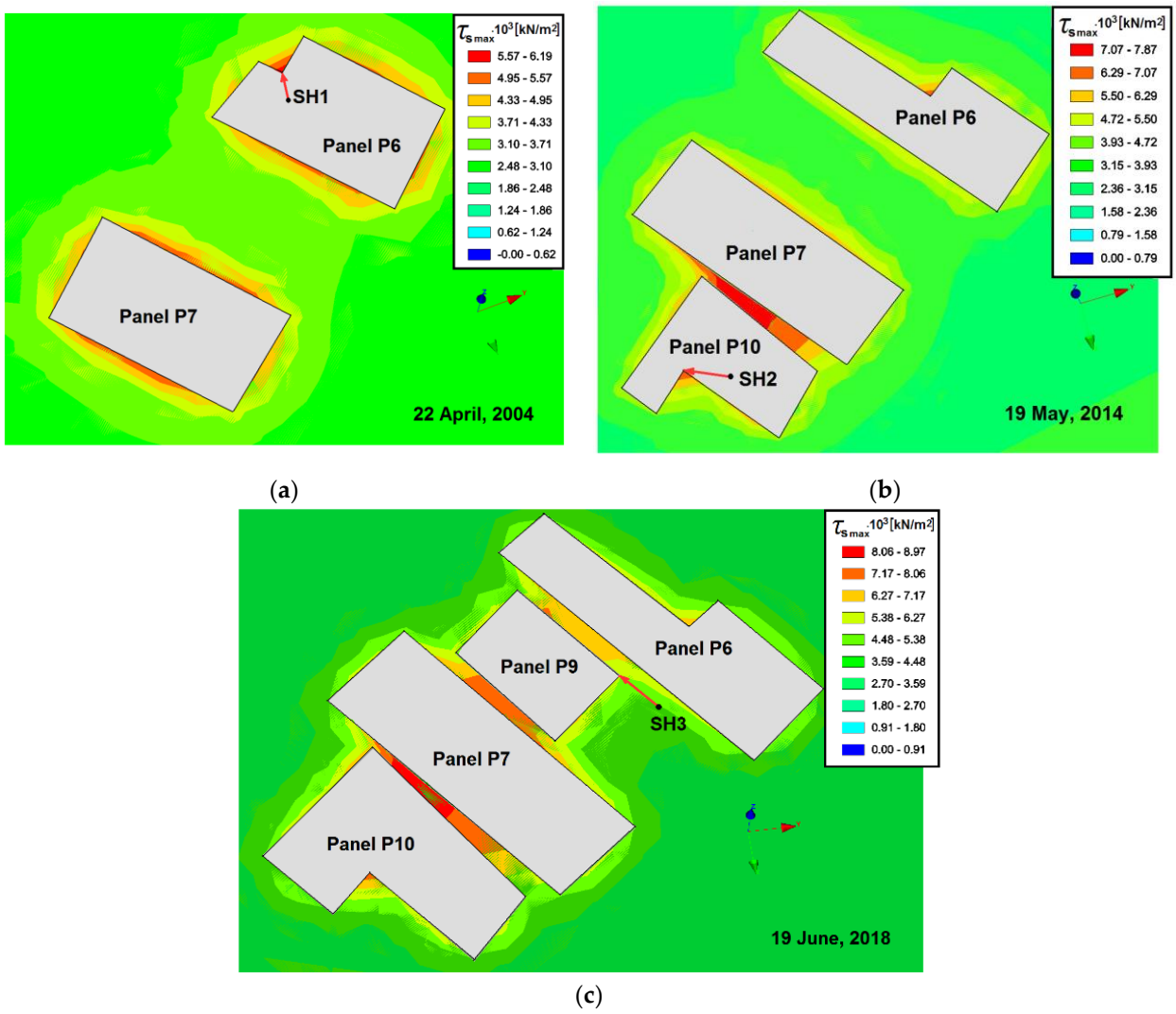



**Figure 17.** Distribution of maximum shear stresses $\tau_{s\,max}$ on the edges of the mining panels, resulting from modeling with 3D finite elements: (**a**) the model dated 22 April 2008; (**b**) the model from 19 May 2014; (**c**) the model from 19 June 2018.

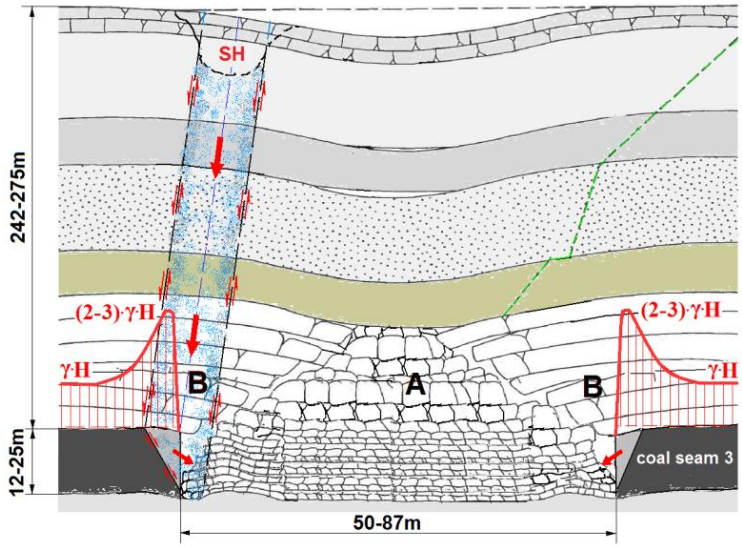



**Figure 18.** Behavior of rocks in a vertical cross-section on the mining panels (modified after Lee & Abel [45]).

6.2.1. The Phenomenon of Subsidence Terraces/Discontinuity Steps

The phenomenon of subsidence terraces or subsidence discontinuity steps is characteristic of the areas in the middle of the panels, from the limit with faults (such as the subsidence terrace T4—Figure 12) or as a temporary phase, preceding the formation of sinkholes, near the edges of the pillars between the panels (as is the case of the T3 subsidence terrace—Figure 16a).

In the areas in the middle of the mining panels, the rocks collapse, forming caving vaults with a height of approximately 120–150 m, which do not reach the ground surface and whose upper limit is located at a distance of over 100 m from the surface. If there had been no tectonic accidents at the limit with the pillars of the mining panels, the collapse of the rocks would have propagated to the surface, following the limit plan of subsidence or movement of the rocks, with an inclination of approximately 55–60° from the horizontal, leading to the formation of continuous troughs. The height of the caving vaults, generated by the massive exploitation by the longwall top coal caving method, was large enough to reach the fault plane and trigger the phenomenon of subsidence terraces. In this particular case, the movement of the rocks was limited by the first F1 fault, then continued to the surface on contact with the second F2 fault, propagating only in the rock block below the fault (see Figure 19). The rocks block below the fault suffered gravitational downward movements so that the fault plane was subjected to shear stresses, followed by a shear displacement, which can be expressed by the Mohr–Coulomb law: (where $\tau_{fault}$ are the shear stresses on the fault plane; $\sigma_{n\ fault}$—normal fault stresses; $c$ is the fault cohesion; $\phi$—the internal friction angle on the fault plane; $R_{s\ fault}$—shear strength of the fault plane). Considering the presence of coal faces below the fault plane, which produced the undermining of the faults so that tensile stresses were transmitted to the plane of the faults, which tended to detach the rock block below the fault from the upper one, according to the condition: $\sigma_{t\ fault} \geq R_{t\ fault}$ (where $\sigma_{t\ fault}$ is the normal tensile stresses on the fault; $R_{t\ fault}$—the tensile strength of the fault plane).

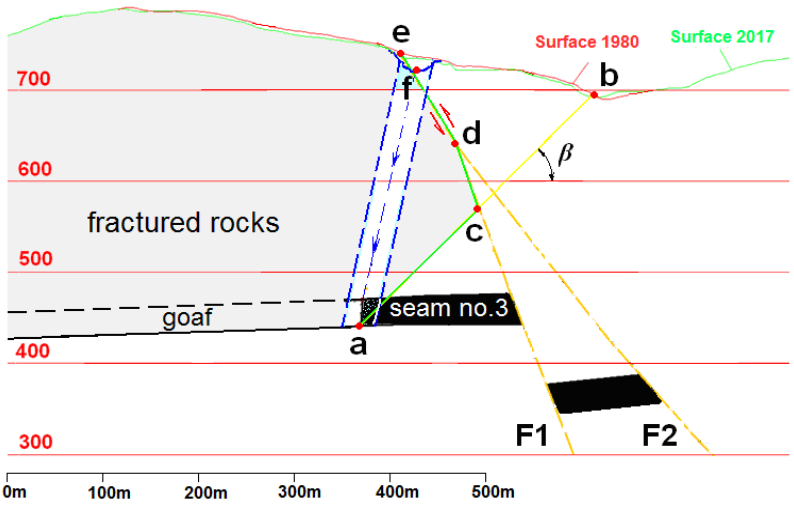



**Figure 19.** Mechanism of sinkholes formation following the exploitation of coal seam no. 3, block V, Lupeni mine. F1, F2—major faults; (**a**,**b**)—the subsidence plane inclined at an angle $\beta$; (**a**,**f**)-sinkhole axis; (**a**,**c**,**d**,**e**)—the delimitation border of the movement of the rocks.

If in the exploitation stage of the panels, the fractured rocks in the caving vault loosened by up to 140–150%, somewhat supporting the block of rock layers above the fault; as time passed, they gradually compressed, entraining the entire rock layer block located above the fault. The wide differentiated displacement of the caved rocks below the fault plane, which sought to fill the void resulting from the exploitation, compared to the lower displacement of the upper rock bank, located in the cantilever and required for bending,

determined the appearance of terraces in the subsidence troughs, at the border with the faults. The development of these phenomena of the appearance of terraces by reactivating faults is very well explained by Donnally et al. [15] for the conditions of coal deposits in the UK.

#### 6.2.2. The Sinkholes Phenomenon

The development of the sinkholes geomechanical phenomenon, until a certain moment, follows the formation mechanism specific to the T3 subsidence terraces (Figure 16a), described above. Basically, the terraces were formed in an area, from the faults limit, where the caved rocks under the faults, by loosening, had the ability to support the block of rocks above the faults. In the case of sinkholes, which occurred at the boundary with the pillars between the panels, the rocks' loosening is not large enough, due to the fact that the rock layers of the immediate roof fracture into large blocks, which rotate towards the goafs, and rocks of the main roof are in the cantilever, on the border with the pillars.

At one point, the stresses concentrated on the corners of the pillars (see Figure 17) exceed the shear strength limit of the roof rock layers, which fracture after a circular or elliptical cylindrical surface and, under the effect of gravity, move downward towards the void produced by the extraction of coal at the limit of the pillars. This is obvious from the situation plans represented in Figure 5, where the axis of the sinkholes makes the connection between the corner of the pillars and the center of the pits formed at the surface.

In Figure 18, the division of the collapsed rocks from the roof, located above the goafs, into two areas can be seen:

- zone A (in the middle of the panels), in which the rocks crumble into smaller pieces, loosen, and tend to fill the voids resulting from exploitation and from their own area of origin—the high loosening coefficient, which can reach 1.5;
- zone B (from the boundary with the pillars), where the rock layers from the immediate roof fragment into large blocks, and those from the main roof form cantilevers oriented towards area A—the low loosening coefficient of approximately 1.1–1.15.

In zone A, the rocks loosen progressively and the movement of the massif is transmitted to the ground surface, causing the formation of continuous deformations of the land to the limit with tectonic accidents that radically change the character of the ground surface movement.

In zone B, due to the concentration of stresses at the boundary with the pillars and the mining edges, the high coal wall (>12–25 m) suffered a coal landslide towards the goaf, causing the formation in the coal seams of slopes with an inclination below 55–60° and implicitly important voids. These slopes led to a reduction in the support of the upper rock layers (located in the cantilever or in the form of large articulated blocks), which, under the influence of excessive stresses in the corners of the panels, suffered failures after a circular or elliptical cylinder, followed by their movement inside the chimney caving, due to the reduction of rocks loosening to less than 5%, under the effect of gravitational forces.

In conclusion, a sinkhole can only be formed if there is a significant void at its base. In this case, part of the void was generated by breaking the corners of the pillars, followed by moving/sliding the fragmented coal towards the goaf and sloping the mining edges (practically, in the corners of the pillars a slope was formed after the two corner planes), and by gravitational compaction of the voids between the upper rock layers (in the cantilever or fragmented), reducing the volume of the voids to a minimum value.

If we aim to stagger the appearance of sinkholes in time, we can conclude that the sinkholes appear only at the border with the panels in the operation phase, being less likely to appear at the border with the panels already exploited where, instead, in the same conditions, there is the possibility of terraces or steps appearing in the subsidence profile, in the outcrop areas of the faults.

If we analyze Figure 5c, we can see that there are almost all the conditions stated for a new sinkhole to appear between panel P9 and panel P7, during the extraction of coal from panel P9. If this were the case, then the latter would have joined with SH3 sinkhole,

producing a huge pit with an elliptical profile, oriented in the direction of the major faults in block V. However, this phenomenon has not appeared until now, due to the de-stressing of the rocks following the collapses that caused the SH3 sinkhole, which exceeded the faults plane, thus bringing an additional contribution of caved rocks from the bank located above the fault, so that only a subsidence terrace occurs on the ground surface, in the fault outcrop, namely the T4 terrace. If followed, on the plane in Figure 17c, the subsidence produced in 2017, on the area of a potential SH4 sinkhole, had a value of 5.1 m.

Figure 19 summarizes the appearance of the sinkholes in the perimeter of the Lupeni mine.

During the top coal caving mining of coal seam no. 3, successively in panels P6, P10, and P9, after a certain distance from the starting line of the coalface (P6: 89.8 m; P10: 102.4 m; P9: 74.1 m), the roof rocks of coal seam no. 3, set in motion by ellipsoids, at each advancement step of 1.25 m, continued their tendency to move along an "ab" subsidence plane, inclined at an angle to the horizontal. However, reaching the plane of the F1 fault, at point "c", they determined the detachment of the rocks on the fault plane, then continued their movement to point "d", where the moving rocks met the plane of the F2 fault, thus deviating the displacement after the inclination of this fault, to the surface, at the outcrop point "e" of the F2 fault. Thus, due to the shearing and detachment of rocks according to the fault planes, the breaking surface marked by the "acde" points delimited a partition wall between the moving rocks (vertical and horizontal displacement), located above the panel in operation and the massif of intact rocks.

If there had been no faults at the boundary with the mining panels, then the rocks in the immediate and main roof would have moved according to the "ab" subsidence plane, loosened progressively, and led to the total movement of the rocks and implicitly to the deformation of the ground surface, where some continuous subsidence would have formed. The presence of faults determined the change of the behavior of the roof rocks, generating the appearance of discontinuous deformations at the ground surface.

## 7. Conclusions

Following the study summarized in this article, it was concluded that the main factors that led to the appearance of the three sinkholes in the Lupeni mining perimeter are the following:

a) shallow depth of underground excavations (below 242–275 m);
b) the displacement of large volumes of rocks from the roof, following the exploitation with LTCC (over 12–25 m);
c) the movement of rock masses according to the fault planes (reactivation of faults), determined by the approach of the mining panels in operation;
d) concentration of stresses on the corners of the panels.

Analyzing the discontinuities that appeared in the subsidence profile, at the limit with the mining panels P6, P9, P7, and P10, two different discontinuity phenomena can be noticed, namely (a) the phenomenon of subsidence terraces and (b) the phenomenon of sinkholes.

The phenomenon of subsidence terraces is characteristic of the areas in the middle of the panels, from the faults limit, or as a temporary phase, predecessor to the formation of sinkholes, near the edges of the pillars between the panels.

The development of the geomechanical phenomenon of sinkholes, until a certain moment, follows the formation mechanism specific to subsidence terraces. Basically, the terraces were formed in an area, from the limit with faults, where the rocks from the block under the fault had the capacity, by loosening, to support the upper block of faults.

In the case of sinkholes that occur at the border with the pillars between the panels, the loosening of the rocks is not enough, due to the fact that the layers of the immediate roof fracture into large blocks that rotate towards the goafs, and those of the main roof are in the cantilever, on the border with the pillars.

The collapsed rocks above the mining panels are divided into two zones: zone A (in the middle of the panels), in which the rocks cave into smaller fragments and loosen,

and zone B (from the boundary with the pillars), where the rock layers of the roof form cantilevers or fragment into large blocks.

A sinkhole can only form if there is a significant void at its base. In this case, part of the void was generated by breaking the corners of the pillars, as a result of the concentration of stresses, followed by the sliding of the fragmented coal towards the goafs; and another part by gravitational compaction of the voids between the upper rock layers (in the cantilever or fragmented), reducing the volume of the voids to a minimum value. The voids created led to the reduction of the support of the upper rock layers, which, under the influence of excessive stresses in the corners of the pillars, suffered failures after a circular or elliptical cylinder, followed by their movement inside the chimney caving, under the effect of gravitational forces.

**Author Contributions:** D.-P.M. generated the DEMs and interpreted the in situ measurements, elaborated the prediction model based on the influence functions method, and realized the numerical models. I.O. conceptualized the numerical models, interpreted the results, and wrote the paper. All authors have read and agreed to the published version of the manuscript.

**Funding:** This research received no external funding.

**Institutional Review Board Statement:** Not applicable.

**Informed Consent Statement:** Not applicable.

**Data Availability Statement:** Not applicable.

**Acknowledgments:** We would like to thank to the management of the Lupeni mine for making available to us the data regarding the underground mining.

**Conflicts of Interest:** The authors declare no conflict of interest.

## References

1. Brady, B.H.G.; Brown, E.T. *Rock Mechanics for Underground Mining*, 3rd ed.; Kluwer Academic Publishers, Springer Science + Business Media, Inc.: New York, NY, USA, 2004.
2. Tajduś, K.; Sroka, A. Analytic and numerical methods of sinkhole prognosis. In Proceedings of the Altbergbau—Kolloquium, Freiberg, Germany, 8–10 November 2007; pp. 152–165.
3. Harms, S.; Konietzky, H. Overburden Subsidence and Sinkholes. TU Bergakademie FREIBERG, Institut für Geotechnik, Updated: 26 October 2020. Available online: https://tu-freiberg.de/sites/default/files/media/professur-felsmechanik-32204/Ebook/28_overburden_subsidence_and_sinkholes_1.pdf (accessed on 15 March 2021).
4. Cabala, J.; Teper, L.; Rutkowski, R. Rockmass deformations caused by zinc and lead ores mining in the Olkusz region (southern Poland). *Acta Geodyn. Geomater.* **2004**, *133*, 47–58.
5. Canbulat, I.; Zhang, C.; Black, K.; Johnston, J.; McDonald, S. Assessment of Sinkhole Risk in Shallow Coal Mining. In Proceedings of the 10th Triennial Conference on Mine Subsidence, Pokolbin, Australia, 5–7 November 2017; pp. 331–347.
6. Kotyrba, A. A study of sinkhole hazard at area of locked colliery. In Proceedings of the Post-Mining Conference, Nancy, France, 16–17 November 2005.
7. Kryzia, K.; Majcherczyk, T.; Niedbalski, Z. Variability of exploitation coefficient of Knothe theory in relation to rock mass strata type. *Arch. Min. Sci.* **2018**, *63*, 767–782.
8. Kryzia, K.; Majcherczyk, T.; Niedbalski, Z. Estimation of mining impact on surface in relation to rock mass type. *Min. Res. Manag.* **2018**, *34*, 151–170.
9. Sałustowicz, A. *Description of Rock Mechanics*; Silesian Publishing House: Katowice, Poland, 1965. (In Polish)
10. Arkuszewski, J. Research on the Determination of the Discontinuous Surfaces Deformation Caused by Shallow Underground Mining. Ph.D. Thesis, Wydział Górniczy, Politechnika Śląska, Katowice, Poland, 1978. (In Polish).
11. Kratzsch, H. *Mining Subsidence Engineering*; Springer-Verlag Publisher: Berlin/Heidelberg, Germany, 1983.
12. Peng, S.; Zhang, J. *Engineering Geology for Underground Rocks*; Springer-Verlag: Berlin/Heidelberg, Germany, 2007.
13. Ekmekci, M.; Yazıcıgil, H. Progressive Sinkhole Occurrence Induced by Dewatering Activities in a Large Lignite Mine (SE Turkey). In Proceedings of the International Mine Water Association, Leipzig, Germany, 11–15 July 2016; pp. 486–493.
14. Bell, F.G.; Donnelly, L.J. *Mining and Its Impact on the Environment*; Taylor & Francis Ltd. Publisher: London, UK, 2015.
15. Donnelly, L.J.; Culshaw, M.G.; Bell, F.G. Longwall mining-induced fault reactivation and delayed subsidence ground movement in British coalfields. *Q. J. Eng. Geol. Hydrogeol.* **2008**, *41*, 301–314. [CrossRef]
16. Cui, H.; Xue, Z.; Jia, X. Reactivated Faults in Mining Area. *Mem. Muroran Inst. Tech.* **2009**, *59*, 101–106.
17. Donnelly, L.J. Predicting the Reactivation of Geological Faults and Rock Mass Discontinuities during Mineral Exploitation, Mining Subsidence and Geotechnical Engineering. Ph.D. Thesis, University of Nottingham, Nottingham, UK, 1994.

18. Parise, M.; Lollino, P. A preliminary analysis of failure mechanisms in karst and man-made underground caves in Southern Italy. *Geomorphology* **2011**, *134*, 132–143. [CrossRef]
19. Lokhande, R.D. An Investigation into the Causes of Pot-Hole Subsidence and its Prediction in Underground Coal Mining. Ph.D. Thesis, ISM Dhanbad, Jharkhand, India, 2013.
20. Marian, D.P.; Onica, I.; Marian, R.R.; Floarea, D.A. Finite element analysis of the state of stresses in the structure of buildings influenced by underground mining of hard coal seams in the Jiu Valley basin (Romania). *Sustainability* **2020**, *12*, 1598. [CrossRef]
21. Sahu, P.; Lokhande, R.D. An Investigation of Sinkhole Subsidence and its Preventive Measures in Underground Coal Mining. *Procedia Earth Planet. Sci.* **2015**, *11*, 63–75. [CrossRef]
22. Galvin, J.M. *Ground Engineering: Principles and Practices for Underground Coal Mining*; Springer International Publishing: Cham, Switzerland, 2016.
23. Govindan, K.; Kannan, D.; Shankar, K.M. Evaluating the drivers of corporate social responsibility in the mining industry with multi-criteria approach: A multi-stakeholder perspective. *J. Clean. Prod.* **2014**, *84*, 214–232. [CrossRef]
24. Andrioni, F. Social-economic influences of mining syncopes in the Jiu Valley over the members of the community. *Ann. Petroşani Univ. Min. Eng.* **2017**, *18*, 178–189.
25. Andrioni, F. *Contemporary Social Work between Theory and Practice*; Academica Greifswald: Rostock, Germany, 2018.
26. Guéguen, Y.; Deffontaines, B.; Al Heib, M.; Fruneau, B.; De Michele, M.; Raucoules, D.; Guise, Y.; Planchenault, J. Detection and characterisation of residual mining subsidence using DINSAR and PS Interferometry: Application to Nord Pas-De-Calais Coalbasin (Northern France). In Proceedings of the Envisat Symposium, Montreux, Switzerland, 23–27 April 2007.
27. Xiong, L.; Wang, G.; Bao, Y.; Zhou, X.; Sun, X.; Zhao, R. Detectability of repeated airborne laser scanning for mountain landslide monitoring. *Geosciences* **2018**, *8*, 469. [CrossRef]
28. Liu, X. Airborne LiDAR for DEM generation: Some critical issues. *Prog. Phys. Geogr. Earth Environ.* **2008**, *32*, 31–49.
29. Singh, M.M. Mine subsidence. In *SME Mining Engineering Handbook*, 2nd ed.; Hartman, H.L., Ed.; Society for Mining, Metallurgy and Exploration, Inc.: Littleton, CO, USA, 1992; Chapter 10.6.
30. Luo, Y.; Cheng, J. An influence function method based subsidence prediction program for longwall mining operations in inclined coal seams. *Min. Sci. Technol.* **2009**, *19*, 592–598. [CrossRef]
31. Luo, Y. An improved influence function method for predicting subsidence caused by longwall mining operations in inclined coal seams. *Int. J. Coal Sci. Technol.* **2015**, *2*, 163–169. [CrossRef]
32. Malinowska, A.; Hejmanowsk, R.; Dai, H. Ground movements modeling applying adjusted influence function. *Int. J. Min. Sci. Technol.* **2020**, *30*, 243–249. [CrossRef]
33. Agioutantis, Z.; Karmis, M. SDPS—Surface Deformation Prediction System for Windows, Version 5.2, Quick Reference Guide and Working Examples, Department of Mining and Minerals Engineering, Virginia Polytechnic Institute and State University Blacksburg, February 2002. Available online: http://update.carlsonsw.com/public/sdps_qref.pdf (accessed on 15 March 2021).
34. Cai, M.; He, M.; Liu, D. *Rock Mechanics and Engineering*; Science Press: Beijing, China, 2013; pp. 32–38.
35. Gao, Y.; Liu, D.; Zhang, X.; He, M. Analysis and optimization of entry stability in underground longwall mining. *Sustainability* **2017**, *9*, 2079. [CrossRef]
36. Marian, D.P.; Onica, I.; Cozma, E. Sensibility analysis of the subsidence parameters at the variation of the main geo-mining factors. *Min. Rev.* **2011**, *17*, 29–35.
37. Onica, I.; Marian, D. Ground surface subsidence as effect of underground mining of the thick coal seams in the JiuValley Bassin. *Arch. Min. Sci.* **2012**, *57*, 547–577.
38. Herget, G. *Stresses in Rocks*; Balkema Publisher: Rotterdam, The Netherlands, 1987.
39. Onica, I.; Chiril, G. *Top Coal Caving Mining in Longwall Faces*; AGIR Publishing House: Bucharest, Romania, 2005. (In Romanian)
40. Onica, I.; Mihailescu, V.; Andrioni, F. Economical optimization of the mechanized longwall faces with top coal caving mining, in horizontal slices. *Arch. Min. Sci.* **2016**, *61*, 651–676. [CrossRef]
41. Le, T.D.; Mitra, R.; Oh, J.; Bruce Hebblewhite, B. A review of cavability evaluation in longwall top coal caving. *Int. J. Min. Sci. Technol.* **2017**, *27*, 907–915. [CrossRef]
42. Wang, Q.; Liu, W.; Lin, X. The Characteristics of the Ground Pressure Manifestation and the Movement of the Top-coal Mass in the Gently Inclined Working Faces with Top-coal Drawing. In Proceedings of the International Symposium on Modern Mining Technology, Shandong, China, 12–14 October 1988.
43. Zhang, D. Strata Control at the Face with Fully Mechanized Sublevel Caving. In Proceedings of the Sixth International Symposium on Mine Planning and Equipment Selection, Ostrava, Czech Republic, 3–6 September 1997.
44. Sidorenko, A.A.; Ivanov, V.V.; Sidorenko, S.A. Numerical simulation of rock massif stress state at normal fault at underground longwall coal mining. *Int. J. Civ. Eng. Tech.* **2019**, *10*, 844–851.
45. Lee, F.T.; Abel, J.F., Jr. Subsidence from Underground Mining: Environmental Analysis and Planning Considerations. Geological Survey Circular 876, United States Department of the Interior, 1983. Available online: https://pubs.usgs.gov/circ/1983/0876/report.pdf (accessed on 15 March 2021).